POLITECNICO DI TORINO
Repository ISTITUZIONALE

Local- and Plot-Scale Measurements of Soil Moisture: Time and Spatially Resolved Field Techniques in Plain, Hill and Mountain Sites

Original
Local- and Plot-Scale Measurements of Soil Moisture: Time and Spatially Resolved Field Techniques in Plain, Hill and Mountain Sites / Raffelli, G., Previati, M., Canone, D., Gisolo, D., Bevilacqua, I., Capello, G., Biddoccu, M., Cavallo, E., Deiana, R., Cassiani, G., Ferraris, S.. - In: WATER. - ISSN 2073-4441. - STAMPA. - Water:9(2017), pp. 21-48. [10.3390/w9090706]

Availability:
This version is available at: 11583/2793514 since: 2020-02-16T23:14:25Z

Publisher:
Water - Open Access Journal

Published
DOI:10.3390/w9090706

Terms of use:

This article is made available under terms and conditions as specified in the corresponding bibliographic description in the repository

Publisher copyright

(Article begins on next page)

19 June 2026

water

MDPI

Article

Local- and Plot-Scale Measurements of Soil Moisture: Time and Spatially Resolved Field Techniques in Plain, Hill and Mountain Sites

Giulia Raffelli [1], Maurizio Previati [1,*], Davide Canone [1], Davide Gisolo [1], Ivan Bevilacqua [1], Giorgio Capello [2], Marcella Biddoccu [2], Eugenio Cavallo [2], Rita Deiana [3], Giorgio Cassiani [4] and Stefano Ferraris [1]

1 Interuniversity Department of Regional and Urban Studies and Planning (DIST), Polytechnic and University of Torino, viale Mattioli, 39, 10125 Torino, Italy; giulia.raffelli@gmail.com (G.R.); davide.canone@unito.it (D.C.); davide.gisolo92@gmail.com (D.G.); Ivan.bevilacqua@gmail.com (I.B.); stefano.ferraris@unito.it (S.F.)

2 Institute for Agricultural and Earthmoving Machines, Italian National Research Council, Strada delle Cacce 73, 10135 Torino, Italy; g.capello@ima.to.cnr.it (G.C.); m.biddoccu@ima.to.cnr.it (M.B.); e.cavallo@imamoter.cnr.it (E.C.)

3 Department of Cultural Heritage (dBC), University of Padova, 35127 Padova, Italy; rita.deiana@unipd.it

4 Department of Geosciences, University of Padova, 35127 Padova, Italy; giorgio.cassiani@unipd.it

* Correspondence: maurizio.previati@unito.it; Tel.: +39-011-0907428

Received: 2 June 2017; Accepted: 11 September 2017; Published: 15 September 2017

Abstract: Soil moisture measurement is essential to validate hydrological models and satellite data. In this work we provide an overview of different local and plot scale soil moisture measurement techniques applied in three different conditions in terms of altitude, land use, and soil type, namely a plain, a mountain meadow and a hilly vineyard. The main goal is to provide a synoptic view of techniques supported by practical case studies to show that in such different conditions it is possible to estimate a time and spatially resolved soil moisture by the same combination of instruments: contact-based methods (i.e., Time Domain Reflectometry—TDR, and two low frequency probes) for the time resolved, and hydro-geophysical minimally-invasive methods (i.e., Electromagnetic Induction—EMI, Ground Penetrating Radar—GPR, and the Electrical Resistivity Tomography—ERT) for the spatially resolved. Both long-term soil moisture measurements and spatially resolved measurement campaigns are discussed. Technical and operational measures are detailed to allow critical factors to be identified.

Keywords: soil moisture measurements; TDR; FDR Sensors; EMI; ERT; GPR; case studies

1. Introduction

1.1. Soil Moisture and Soil–Water Relations

Soil moisture can be defined as the water in the uppermost part of a field soil, and it is strictly affected by soil physical properties, such as texture, organic matter content and stone presence, but also by land cover (vegetation), land use, topography and rainfall [1–3]. Soil moisture represents a key state variable to understand surface hydrological processes (such as drainage, evaporation and plant uptake) and it controls water and energy exchanges between the land surface and the atmosphere [4,5] contributing also, as key factor, in soil–snow interactions and snow gliding [6]. Through direct evaporation and plant transpiration, soil moisture regulates the partitioning of the incoming solar energy at the land surface into the outgoing sensible, latent, and ground heat fluxes. Furthermore, soil moisture plays a significant role in the organization of natural ecosystems and

biodiversity [4], also with consequences for human disease (e.g., malaria transmission [7]). This is especially important in water-scarce environments where more frequent drought events occur [8].

Considering agricultural and irrigation management practices, since soil moisture is extremely variable in space and time, it is very important to accurately evaluate its spatiotemporal dynamics in the root zone at the field scale. In fact, soil water content strongly influences crop production, crop health, and soil salinization. In addition, understanding the factors controlling soil moisture variability allows for an improvement in irrigation management strategies with respect to crop production and optimal use of water resources [5,9,10].

During the last decades new approaches and techniques for monitoring, modelling and using soil moisture data have been developed e.g., [11–13]. With reference to soil moisture monitoring, several studies have been focused on surveying test sites having very different morphological conditions. Lin et al. [1] did year-round monitoring at different sites in the Shale Hills Catchment in central Pennsylvania and found a temporal stability of the soil moisture spatial pattern, which was governed by soil types and landforms. Tromp-van Meerveld and McDonnell [2] measured soil moisture content at different depths between the soil surface and the soil-bedrock and in different locations across the trenched hillslope in the Panola Mountain Research Watershed, GA, USA. They observed that spatial differences in soil depth and total water available at the end of the wet season and during the summer period appeared to be responsible for the spatial differences in basal area and species distribution between upslope and mid-slope sections of the hillslope. Teuling et al. [3] investigated the role of interannual climate variability on soil moisture spatial dynamics for a field site in Louvain-la-Neuve, Belgium, considering three different years (intermediate conditions—1999; wet conditions—2000; extremely dry conditions—2003). They observed that climate variability induces non-uniqueness and two distinct hysteresis modes in the yearly relation between the spatial mean soil moisture and its variability.

In this work we show the soil moisture estimation at local and plot scale in three different field conditions: a plain permanent meadow, a mountain permanent meadow and a hilly vineyard (all located in Northwestern Italy). The main goal is to provide a synoptic view of techniques supported by practical case studies to show that in very different conditions it is possible to estimate a time and spatially resolved soil moisture by the same combination of instruments: contact-based methods for the time resolved, and minimally invasive hydro-geophysical methods for the spatially resolved. Both long-time measurement series and single-measurement campaigns performed simultaneously with different techniques are presented.

The paper is organized as follows. In the following part a general overview of the field measurement technique is presented. In Section 2 we describe some of the available measurement techniques (also employed for the purpose of this paper) to evaluate soil water content both at the local and at the plot scale, focusing on how they work from a theoretical point of view. In Section 3 we present three different case studies (together with the obtained results), showing how we applied the methods. In Section 4 we discuss the results. In Section 5 we draw conclusions and provide an outlook on current opportunities and challenges.

1.2. Soil Moisture and Field Measurement Techniques: A General Overview

According to Robinson et al. [11], soil moisture in situ measurement methods can be divided into contact-based and contact-free methods. Contact-based methods imply direct contact with the soil. They are mostly applied at the local scale, and include both the destructive sampling (e.g., gravimetric methods—also defined as properly "direct" method—[14]), and indirect methods that account for the effects exerted by water content in the soil on its dielectric properties such as: Time Domain Reflectometry—TDR e.g., [15–17]; Frequency Domain Reflectometry—FDR e.g., [11]; capacitance sensors e.g., [18,19]; and Time Domain Transmission (TDT) sensors, e.g., [20]. The sensor networks (wireless in particular) are generally constituted by capacitance, FDR, and TDT sensors, e.g., [5,21,22]; however, more complex but reliable solutions are represented by TDR multiplexing systems, e.g., [23,24],

similar to the one presented in the plain permanent meadow case study. These techniques give spatially and resolved temporally highly measurements at the local scale (e.g., vertical soil moisture profile) and the spatiotemporal dynamics of soil water content at the field scale [4,25]. Contact-free methods include hydrogeophysical methods and remote sensing. Hydrogeophysical methods provide multi-point measurements using electromagnetic soil moisture sensors, with a spatial resolution down to several meters [5]. The most used hydrogeophysical methods are: (1) Ground Penetrating Radar (GPR) e.g., [26–32], in which the propagation velocity of high frequency (1 MHz to 1 GHz) electromagnetic waves is used to determine the soil dielectric permittivity and thus soil moisture content. It can be used with different setups, such as crosshole, air-launched and surface-based [5,26]; (2) Electromagnetic Induction (EMI) e.g., [33–35], and Electrical Resistivity Tomography (ERT) e.g., [32,35–40], which measure the apparent electrical conductivity (EC_a) of the soil, and will be treated more in detail in the following chapters. Note that strictly speaking ERT is rather a non-invasive method, as galvanic contact with the ground must be ensured. Remote sensing methods include: (a) passive microwave remote sensing e.g., [5,41–43], in which radiometers measure the thermal radiance emitted from the earth surface of a bare or cropped soil, using frequencies between 1 and 12 GHz (L- to X-band), obtaining the dielectric permittivity [5]; (b) airborne and spaceborne active microwave remote sensing (i.e., radar), such as TerraSAR-X, European Remote Sensing 2 (ERS-2), Advanced Synthetic Aperture Radar (ENVISAT/ASAR), Radarsat 2, and Phased Array type L-band Synthetic Aperture Radar (ALOS/PALSAR), which estimate surface soil moisture by the interpretation of the backscattering coefficient (expressed in decibels and depending on the dielectric permittivity of soil and surface roughness) [44,45]; (c) a cosmic-ray probe [46,47], which counts secondary fast neutrons near the soil surface created by primary cosmic-ray particles in the atmosphere and in the soil. The cosmic-ray probe was applied in different environmental and agricultural settings, e.g., [48–50]. Despite effortz, e.g., [51–54], to downscale the remote sensing soil moisture products (from several km to the local scale), the promising results obtained in scale root-zone soil moisture, e.g., [55–58], and the challenging opportunities offered by the future missions under launch in the coming decades, e.g., [59], remote sensing methods have typically been used to detect surface and near-surface soil moisture (topsoil—0–0.05 m) with coarse spatial and temporal resolution. Extensive reviews of these topics are offered by Peng et al. [60] and Mohanty et al. [61]. Within this context, a cosmic-ray probe is actually the only one used at the field scale, because it has the ability to measure integral soil moisture content with an acceptable temporal resolution [5]. However, it is essential to highlight that (i) the cosmic ray footprint radius is some hundreds of meters depending on the humidity, soil moisture and vegetation; (ii) the detector is extraordinarily sensitive for the first few meters close to the detector; and (iii) the penetration depth (on the order of a few decimetres) decreases exponentially with the distance to the sensor, e.g., [46,62–64].

In the following sections we will describe in more detail the soil measurement methods we adopted in our experimental sites. Namely: TDR and two different low-frequency types of soil moisture sensors (ECH_2O—5TM (Decagon Devices Inc., Pullman, WA, USA) and CS616 (Campbell Scientific Inc., Logan, UT, USA)) directly connected to data loggers, which give local measurements of soil water content in time and space; and EMI, GPR, and ERT, which represent plot-scale measurement techniques.

2. Soil Moisture Field Measurement Methods: A Focus on the Techniques Used

2.1. Time Domain Reflectometry (TDR)

As it is non-destructive and less time-consuming with respect to gravimetric measurements, Time Domain Reflectometry (TDR) is a widely used method for soil moisture measurement. Thanks to the accurate results achievable, together with its applicability to a large range of soils and settings, TDR progressively strengthened its position, replacing in the end the gravimetric technique [13]. In this work, a Tektronix 1502 C TDR cable tester coupled with two wire rods probes has been used.

TDR estimates the apparent dielectric permittivity of the soil by measuring the travel time a step voltage pulse takes to propagate along the probe and back. The probe must be placed in the soil either vertically or horizontally at the selected measuring depth. The dielectric permittivity of the system that surrounds the probe depends, in turn, on the soil moisture [65–67]. Calibration requirements are minimal (in many cases soil-specific calibration is not needed), but soil-specific calibration is possible for applications that demand high accuracy.

Once a soil permittivity value has been calculated starting from the travel time measurements, the soil moisture can be obtained by employing either empirical relationships [15] or quasi-physically based equations [68,69]. Considering that soils can have rather different electrical properties, the choice of the proper relationship/equation is connected with the physico-chemical characteristics of the surveyed material.

Different types of TDR field probes were studied in the literature, e.g., [70–77]. Robinson et al. [17] indicated the probes with two parallel rods as those to be preferred in field conditions, since they investigate a bigger volume in a more homogeneous way. Probes with two parallel rods can also be inserted more easily into the soil. Nissen et al. [78] suggested that a balun transformer could be omitted due to the results they obtained in their study.

2.2. Soil Moisture Sensors Directly Connected to Data Loggers

An increasing number of soil moisture sensors directly connected to data loggers are deployed to measure volumetric soil water content (θ) for agricultural, ecological, and geotechnical applications. While time-domain reflectometry (TDR) and transmissometry (TDT) operate at GHz range frequencies, the above mentioned sensors generally operate between 20 and 300 MHz [79]. With respect to time domain techniques, lower-frequency sensors are less expensive and, despite TDR still being more accurate, modern electronics coupled with a better understanding of the theory progressively improve low-frequency sensors' performance [80]. In this work, we present two contact-based sensor types: ECH$_2$O—5TM capacitance/frequency domain sensors (Decagon) and CS 616 water content reflectometers (Campbell Scientific). The frequency of 70 MHz at which both sensors are operating minimizes textural effects (and salinity) [81–83].

ECH$_2$O—5TM sensors employ a capacitance technique to determine soil moisture. In particular, these sensors determine the dielectric permittivity of the medium by measuring the charge time of a capacitor, using the soil as a dielectric medium. CS616 measures a period value. The period in air is approximately 14.7 microseconds, and the period in saturated soil with porosity equal to 0.4 is approximately 31 microseconds. The output is a ±0.7 volt square wave with the frequency dependent on water content. This frequency is scaled down in the water content reflectometer circuit output to a frequency easily measured by a data logger. The probe output frequency or period is empirically related to water content using a calibration equation. Concerning the geometry, 5TM probes have three flat 52 mm long prongs spaced 5 mm apart, while CS616s have two 300 mm long rods with a diameter of 3.2 mm, spaced 32 mm apart. Measurement rods of CS616s are therefore approximately six times longer and six times wider apart than those of 5TMs. With reference to the porous medium measurement volume, considering that it is restricted to the direct surroundings material of the prongs/rods, the 5TMs investigate a soil volume much smaller than the CS616 [82,84]. Particular attention must be paid to the probe–soil contact.

2.3. Electromagnetic Induction (EMI)

As already mentioned, soil is a three-phase (solid–water–air) system, in which the main conducting phase is the aqueous solution. Due to this assumption, apparent Electrical Conductivity (EC_a) measurements can be used to evaluate soil water content [85]. Friedman [85] also states that there are three main categories of factors that can affect soil EC_a: (i) factors describing the bulk soil and the respective volumetric fractions occupied by the three phases and possible secondary structural configurations (aggregation): porosity, water content and structure; (ii) factors quantifying solid particle,

which are relatively time-invariable: particle shape and orientation, particle size distribution, cation exchange capacity (CEC) and wettability; (iii) factors representing soil solution attributes, changing quickly in response to alterations in management and environmental conditions (e.g., environmental factors): ionic strength, cation composition and temperature. Electrical resistivity thus can change in space and time as an effect of (a) lithology (time-independent); (b) moisture content; and (c) pore water salinity. This is accounted for in all constitutive models describing the dependence of bulk electrical resistivity on soil parameters and state variables, starting with Archie's law [86]. The possible misleading effects must be accounted for, as shown in a number of recent literature reports, e.g., [87]. The same problem applies of course to EMI and ERT (see next section) as both measure electrical resistivity/conductivity.

Since it is a fast, non-invasive technique easy to use in field conditions, Electromagnetic Induction (EMI) is often used to map soil properties [88], but also soil moisture changes [35]. EMI follows the principle that within a time-varying electromagnetic field, any conductive object carries a current. Each instrument has two coils, a transmitter and a receiver, placed at either a fixed or variable spacing. Vereecken et al. [5] report typical fixed coil separations between 0.3 and 4.0 m, and a frequency operational range of between 5 kHz and 50 kHz.

EMI induces an electrical current into the soil; the depth of penetration is influenced by the separation of the coils and by the frequency of the current. Since EC_a is affected by soil's properties, the signal reaches a specific depth, also related to the uniformity of the soil. If the soil is very conductive close to the surface, then the signal will be locally dissipated without going deeper. Therefore, the depth of investigation of EMI equipment depends on four principal factors: (1) the resistivity of the investigated soil; (2) the coil separation of the instrument; (3) the coil orientation (vertical or horizontal); and (4) the waveform frequency. By varying the conditions of (2), (3) and (4), multiple depths of investigation can be achieved. The depth of investigation can be obtained as a function of the waveform frequency, the magnetic permeability and the electrical conductivity.

Advanced inversion techniques hold the potential of being applied effectively on small-scale EMI data, such as described above, e.g., [89,90]. While this is not yet common practice for soil moisture monitoring, some notable applications already exist, e.g., [91]. A recent review of EMI methods for hydrological and environmental applications is given by Boaga [92].

A number of EMI instruments are available in the market. For this study, we used a commercial GF Instruments CMD1 system (GF Instruments, Brno, Czech Republic) as well as a commercial GSSI Profiler EMP-400 (Geophysical Survey Systems Inc., Nashua, NH, USA). No inversion was carried out in this study, and maps show apparent electrical conductivity as traditionally estimated using a small induction number approach [93].

2.4. Electrical Resistivity Tomography (ERT)

The ERT is a non-destructive, cost-effective, indirect method that can also acquire data concerning soil moisture data within the subsurface, e.g., [5,40,94,95]. ERT uses a set of electrodes: two that inject electrical current into the soil, and two others that monitor the resulting voltage difference. Given a certain number of deployed electrodes, a very large number of measurement combinations is possible, giving rise to the measured dataset. Different configurations are possible, with pros and cons [94]. The measured voltage differences versus injected currents are summarized in terms of the relative ratio, i.e., the measured resistances (one for each measurement quadripole). A good practice consists of collecting both direct and reciprocal resistances (i.e., swapping current and voltage electrode pairs). Theoretically the two configurations shall give the same resistance value, so differences can be taken as an estimate of measurement error, to be used later for a more educated inversion procedure, e.g., [96]. Data are then inverted to give an estimate of the electrical resistivity spatial distribution that causes the observed resistances. Inversion requires the minimization of the overall difference between measured and simulated resistances, the latter being modelled using a physico-mathematical simulator that reproduces a DC current in a heterogeneous medium. This least-squares approach

must generally be supplemented by some form of regularization [94], i.e., some a priori information about the spatial variability of electrical resistivity. In the most common case, the smoothest spatial distribution is sought, according to the so-called Occam's inversion approach that makes use of error estimates derived, e.g., from reciprocal analysis [94–97]. The resolution of the resulting resistivity distribution estimates decreases with depth, but is also dependent on the resistivity values themselves. The resulting distribution is generally reconstructed in 2D, but 3D imaging is possible if dense electrode distributions are available in 2D at the ground surface or in boreholes [5].

In order to reconstruct soil moisture patterns from ERT data, petro-physical relations such as Archie's law are used [40,98]. ERT measurements are widely employed to monitor vadose zone water dynamics, e.g., [32,94,99,100]. Since ERT allows providing images of spatial scale soil water content variability along either 2D transects or 3D soil volumes (considering high spatial resolution and daily temporal resolution) [5], it has been widely used in the studies of root water uptake by plants and temporal and spatial variations of soil–moisture interactions, e.g., [5,35,101–103]. However, there is evidence that this inversion procedure can produce mass balance errors due to a rapid decrease of ERT resolution with depth [40]. This problem may be solved through a coupled hydro-geophysical approach [40,101]. However, if only qualitative assessment of spatial distribution and time variations of soil moisture content are sufficient, an uncoupled approach can be used [32] based on the following steps: (1) inversion of geophysical field data gives the spatial distribution of electrical resistivity; (2) application of a petro-physical relationship to obtain an estimation of moisture content distribution from the electrical resistivity.

Many ERT instruments are commercially available. In this study we used a commercial IRIS Instruments SYSCAL Pro 10 resistivimeter with 72 channels (IRIS Instruments, Orleans, France). Inversion was carried out using the freely accessible inversion codes developed by Andrew Binley [32,104–106].

2.5. Ground Penetrating Radar (GPR)

GPR is a non-invasive and non-destructive geophysical method that uses radar pulses to image the subsurface. Given that the velocity of an electromagnetic wave in a soil is connected to its bulk dielectric constant (which is, in turn, related to the soil moisture), over the last three decades GPR has also been widely applied to estimate soil moisture in the unsaturated zone. A transmitter emits pulses (high-frequency radio waves typically in the range between 10 MHz and 2.6 GHz) that travel in the medium; when pulses encounter materials having different permittivities they are reflected, refracted or scattered back to the surface where a receiving antenna records the signal. Due to the frequency-dependent attenuation, lower frequencies lead to higher soil depth penetrations. However, higher frequencies provide higher resolutions. Two classes of GPR methods to estimate soil moisture can be distinguished: single-antenna separation methods (from scattering objects and traditional GPR sections), and different antenna separation methods (which require multiple measurements). For a comprehensive presentation of each single method, Huisman et al. [26] provide a detailed review.

Considering that the use of GPR systems is difficult in uneven irregular areas, an application is here presented in the plain permanent meadow case study. A commercial PulseEkko Pro radar system (Sensors and Software Inc., Mississauga, ON, Canada) with 100 MHz antennas has been used. For more details please refer to Rossi et al. [32].

3. Results: Testing Sites Description

In this section we describe the main characteristics of the three experimental sites together with the field campaigns layouts and the measurement methods applied in each site. All sites are located in Northwestern Italy. However, they are representative of very different conditions: the first is a permanent meadow located in a plain, while the second is a meadow located in a sloping mountain

abandoned pasture; finally, the third is a vineyard in a hilly zone. A synoptic scheme of the different equipment used in the different testing sites is given in Table 1.

Table 1. Synoptic table summarizing the different equipment used in the different testing sites.

	Plain [Permanent Meadow]		Mountain [Permanent Meadow]		Hill [Vineyard]	
	Long Time Surveys	Single Campaigns	Long Time Surveys	Single Campaigns	Long Time Surveys	Single Campaigns
Time Domain Reflectometry (TDR)	√	√		√		√
Soil moisture sensors directly connected to data loggers			√		√	
Electromagnetic Induction (EMI)				√		√
Electrical Resistivity Tomography (ERT)		√		√		
Ground Penetrating Radar (GPR)		√				

Authors make the datasets collected within this work available. Readers or researchers interested in receiving and/or analysing one or more dataset shown in this work must address their specific request to the corresponding author.

3.1. Plain Permanent Meadow

Site and instrumental description. The experimental site is located in Grugliasco (Torino), in the northwestern part of the Po Plain, Italy (45°03′ N, 7°35′ E) at 290 m a.s.l. (Figure 1). In this area, rainfall climatology is characterized by two maxima, respectively in spring (April–May) and fall (October–November), and by a relatively dry winter and summer [107,108]. The vegetation growing season lasts, approximately, from late March to mid-October. The monitored area is 1500 m^2, constituted by a permanent meadow. The soil is loamy–sand to sandy (≈80% of sand [32], which progressively rises to ≈95% below the 1st meter), without any gravel, and with a slope of about 1%. These last conditions are particularly suitable for TDR and GPR applications for both practical operation simplification (e.g., TDR probes insertion; GPR surveying process) and porous medium characteristics (i.e., low signal attenuation) e.g., [109,110].

Figure 1. Experimental site located in Grugliasco (Torino–Italy) and a picture shot in April 2005.

Long-term soil moisture measurements. The soil water content monitoring station is based on a TDR Tektronix 1502C and a personal computer controlling 11 multiplexers connected to 160 probes vertically inserted into the soil. The great number of installed probes was conceived to consent the calibration of the 3D numerical codes described by Paniconi et al. [111]. The sandy soil and the absence of stones allowed the vertical insertion without disturbance and/or induced lack of contact. Probes are made out of two parallel stainless steel rods (diameter 6 mm) with the following lengths: 150, 300, 600,

1000 and 2000 mm. To prevent geometrical probes = deformations and keep rods parallel during the insertion process, a steel guide was used. The TDR probes' layout in the experimental field is depicted in Figure 2.

The measurements started in 1997 and, since summer 2005, the TDR measurements have been automatic. The TDR signals are sampled and acquired using WinTDR software [112]. Volumetric soil water content is computed using the composite dielectric approach described by Roth et al. [68]. This relation has been validated by comparison with gravimetric sample measurements in the oven, obtaining an average error of 2%. The sampling time interval between TDR measurements can vary from one hour (during and after rainfall events, or during intense exfiltration periods) up to one day. In the same field, a meteorological station collects meteorological data at hourly intervals.

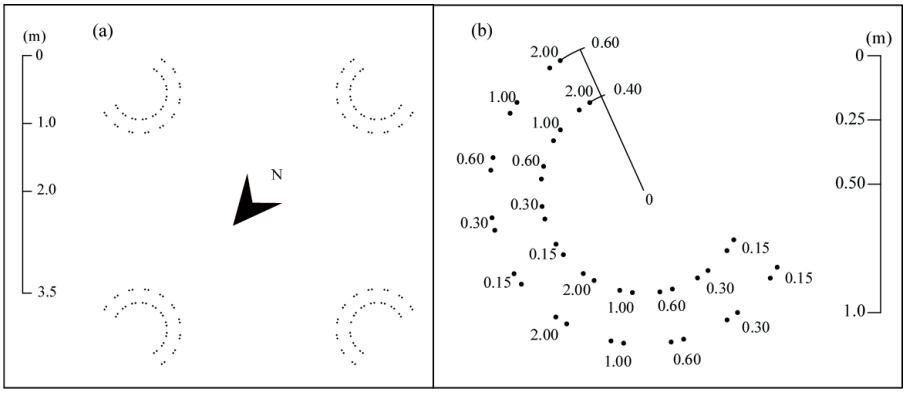

Figure 2. Grugliasco site. (**a**) Layout of the TDR probes in the experimental field; and (**b**) detail of the disposition of the probes of different lengths within one of the four groups.

ERT, GPR and TDR single measurement campaign. To evaluate the soil moisture evolution along time and space, on 28 August 2009 an infiltration experiment (over a rectangular area of 18 m by 2.6 m) was performed at the Grugliasco site. The scheme and a picture of the experimental setup is shown in Figure 3 (for details, see Rossi et al. [32]).

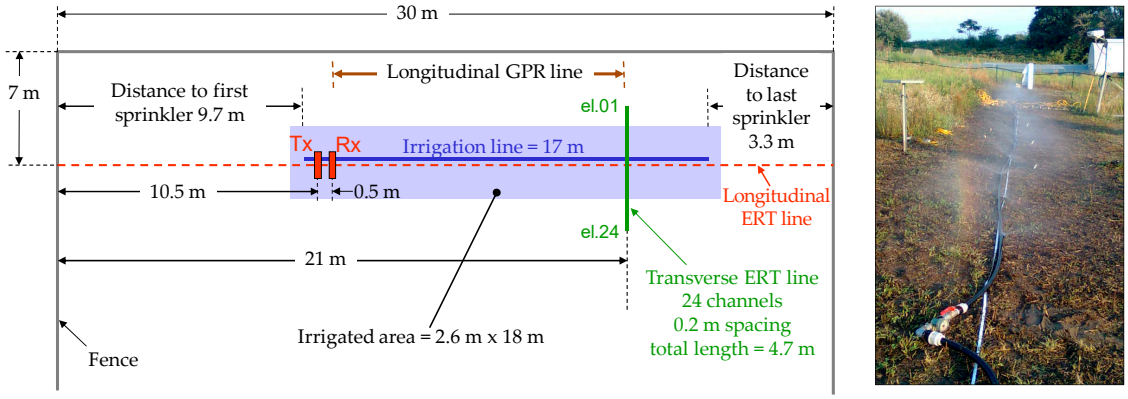

Figure 3. Grugliasco site, August 2009. Scheme of the irrigation experiment setup and a picture taken during the experiment.

The irrigation was performed in three steps: about 2.5 m^3 of water were distributed during the first irrigation step and about 1.5 m^3 during the others. ERT acquisitions occurred during irrigation breaks and with a precise scheduled time. Eight TDR probes with a length of 0.30 and 2.00 m were also vertically inserted into the soil, along the sprinkler line centred on the ERT profile. The absence of ponding was guaranteed by ensuring that the irrigation intensity was always lower than the soil infiltration capacity.

A longitudinal ERT line was acquired along the transect—see Figure 3 for the location—and measurements were taken only before and after irrigation. The line is composed of 48 electrodes with 0.6 m spacing, for a total length of 28.2 m. A dipole–dipole skip zero scheme was acquired, e.g., [113]

3.2. Mountain Permanent Meadow

Site and instrumental description. The Cogne Valley is a side valley of Valle d'Aosta (Northwestern Italy). The experimental site (45°36′ N, 7°21′ E) is located at 1730 m a.s.l. on a 26° slope facing south–southeast (169°)—Figure 4. The vegetation is characterized by herbaceous and shrub components typical of degraded pastures at high altitudes (e.g., *Hippophaë rhamnoides* L.), therefore it is representative of wide areas in the Alps (here, the pastures were abandoned due to the slope and low accessibility). This region is characterized by rainfall occurring mainly in the spring and autumn, with an average of 650 mm per year. The average annual temperature is about 4 °C. The soil depth ranges from 0.4 to 1.5 m, with a sandy loam texture and some gravel (≈73% of sand).

The experimental site is characterized by intense direct solar radiation due to its aspect, resulting in large daily temperature variations. The incident radiation accelerates snow melt and the drying of soil (compared to the plain).

Figure 4. Experimental site located in Cogne (Aosta–Italy) and a picture shot in October 2016.

Long-term soil moisture measurements. Soil water content is measured with three CS616 sensors (Campbell) connected to a CR1000 Data logger. In 2010, data were collected hourly by one probe horizontally inserted at 0.1 m depth. In 2015 two more CS616 probes horizontally inserted into the soil at 0.2 and 0.4 m depths were installed. The gravimetric calibration method and temperature correction were adopted.

EMI, ERT and TDR measurement campaigns. EMI surveys aiming at mapping the spatial and temporal variability of soil resistivity along the steep mountain meadow testing site were performed in 2010, on the 26 September and the 23 October.

Data were collected using a GF Instruments CMD1 in high penetration mode (hence the estimated investigation depth ranges from the surface down to −1.5 m). During the same investigation dates, an ERT survey was performed along a transect located on the slope. A dipole–dipole skip zero acquisition scheme, with full reciprocal acquisition, was adopted. Data were inverted using an Occam inversion approach, as implemented in the Profile R/R2/R3 software package, accounting for the error level estimated from the data themselves [114]; here 5% was chosen as a relative error. During the 26 September 2010 EMI and ERT monitoring campaigns, soil moisture values were also measured by vertically inserted TDR probes. Two transects were investigated: the first was realized with measurements at the beginning, at the centre and at the end of the ERT transect (0.75 m long TDR probes vertically inserted into the soil); the second was more superficial (0.15 and 0.30 m long TDR probes vertically inserted into the soil), conducted perpendicularly to the ERT profile.

3.3. Hilly Vineyard

Site and instrumental description. The "Tenuta Cannona" (44°40′ N, 8°37′ E, 296 m a.s.l.) is located in Carpeneto (AL), 85 km southeast of Torino, Northwest Italy (Figure 5). The area is in the Alto Monferrato hilly region, which is a valuable vine-growing and DOC (Controlled Designation of Origin) wine production area. The soil has a clay to clay–loam texture (≈35% of clay and ≈40% of silt). The climate presents an average annual precipitation of 965 mm (based on the Ovada meteorological station data), mainly concentrated from October to March. Mean annual air temperature measured at the experimental site in the period 2000–2013 was 13 °C and the average annual precipitation was 849 mm [115,116].

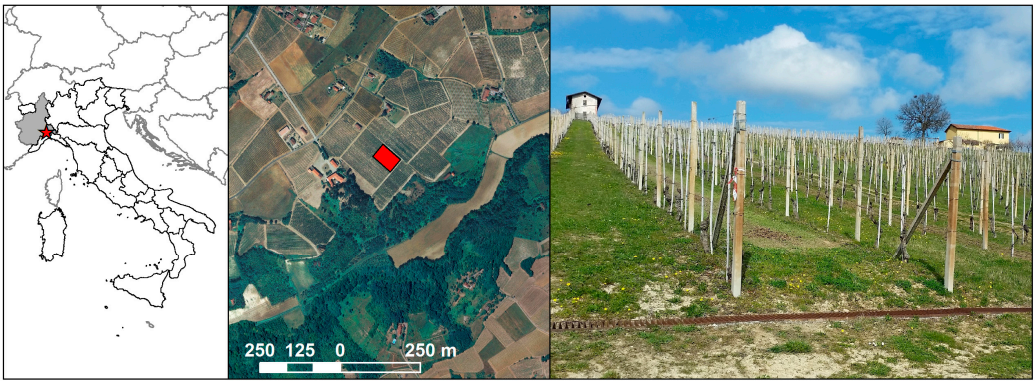

Figure 5. Experimental site located in Carpeneto (Alessandria–Italy) and a picture shot in March 2016.

Long-term soil moisture measurements. A continuous monitoring was performed starting from August 2011 to provide information about the space–time variability of hydrological processes with different cultivation techniques. The test sites, which include conventional tillage ("TI") and grass-covered soil ("GC"), are adjacent to each other on a parcel located on a hill with a SE aspect and average slope of 15%. Each site includes six vine rows aligned along the slope, where the vines are spaced 1.0 m along the row and there is 2.75 m between the rows (Figure 6).

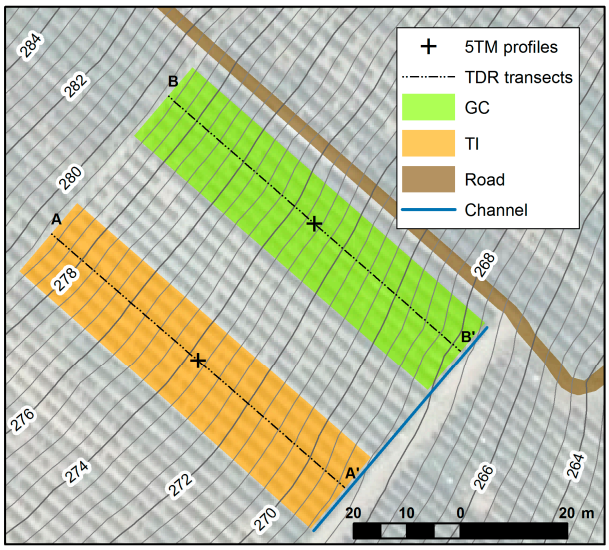

Figure 6. Carpeneto site. Plot of the experimental field. Grass Cover (GC) and Conventional Tillage (TI) represent the two investigated cultivation techniques. The two dotted lines A–A′ and B–B′ represent the investigated TDR transects.

Soil moisture data were collected by measuring the soil dielectric constant using four series of 5TM capacitance probes. Sensors have been horizontally inserted both in the central part of the inter-row

(no soil compaction due to the passage of tractors—"NT") and in the track position ("T"), affected by the passage of tractor wheels. During the monitored period (winter 2015–2016), the soil was never frozen.

As regards to the sensors, we followed the calibration suggested by Decagon Devices which apply the Starr and Paltineanu approach [117], and resulting in an accuracy of ± 0.03 m^3/m^3 ($\pm 3\%$ VWC). Measurements are recorded and stored by a Decagon EM50 Data logger every 60 min.

EMI and TDR combined campaign. In this field campaign, we used the EMP400 multi-frequency EMI sensor, which can collect data up to three frequencies from 1 to 16 kHz, in horizontal dipole orientation (HDO) and vertical dipole orientation (VDO), with a coil spacing equal to 1.22 m. In this study, the EMP400 was used in VDO operating mode, with selected frequencies of 5, 10, and 15 kHz. The EMP400 is very sensitive at greater depths because of the larger coil distance. The EMP400, equipped with an integrated WAAS GPS, was carried by hand.

The TDR soil moisture was detected by a TDR Tektronix 1502C with three probes (made out of two parallel stainless steel rods with diameter 6 mm) vertically inserted into the soil from the surface down to the following depths: 0–0.15 m, 0–0.30 m, and 0–0.75 m. Measurements were performed every 10 m along two transects both in conventional tillage (TI), and in grass cover (GC) rows.

4. Results: Measurement Campaigns and Surveys Outputs

4.1. Plain Permanent Meadow

Long-term soil moisture measurements. The long-time survey depicted in Figure 7 shows the soil moisture data from 1 January 2004 to 31 December 2006 at the following vertical depths: 0–0.3, 0–0.6, and 0–1.0 m. Values are obtained through the arithmetic average of all the probes with the same rod lengths (namely, 16 probes per each considered length).

During the whole of 2004, until summer 2005, measurements were collected on a weekly base. Despite the general agreement with the precipitation data, the weekly sampling time is not exhaustive in terms of hydrological processes description (especially with coarse texture soils characterized by fast dynamics). Under such condition, minor meteorological events characterized by low magnitudes, are often not detected by the soil moisture profiles. At the same time soil moisture peaks corresponding to high precipitation events appear often damped (i.e., rarely exceeding the 0.20 m^3/m^3). Starting from August 2005, data have been automatically collected at hourly steps. With this sampling interval, minor events are also detected, and soil moisture peaks are better described, arriving to reach at the 0.30 m^3/m^3 threshold (which can be considered close to saturation for the investigated sandy soil).

With reference to the adopted experimental set-up, characterized by TDR probes vertically inserted into the soil, all the different lengths of probes react to meteorological forcing. Obviously this reaction is inversely proportional to the investigated soil volume/layer in relation to the magnitude of the events (both in terms of wetting and drying). Accordingly, the most intense reaction is observable in the data collected by the shortest probes (in Figure 7 represented by the 0.30 m lengths), which investigate the shallowest layer. Moreover, during the winter months, the presence of frozen topsoil can lead to TDR measurement complications due to the TDR's inability to detect simultaneously liquid and ice contents in frozen soils within the bandwidth included between a few megahertz and 1.5 GHz [118,119]. These complications, if not properly considered, can cause measurement errors proportional to the soil depth reached by the frost in relation to the depth investigated by the probes.

ERT, GPR and TDR single measurement campaign. Figure 8 shows how visible is the patch of soil where irrigation had taken place with respect to the non-irrigated zone. However, at this measurement scale, it is hard to identify the depth of infiltration as the resolution cannot be any better (and is actually worse) than the electrode spacing (0.6 m in this case).

In order to capture in more detail the changes in moisture content with depth, ERT measurements were collected also using 24 electrodes (spaced 20 cm), set on a transect perpendicular to the sprinkler's line over a total length of 4.6 m. Surface data were obtained with a Syscal-Pro resistivimeter (IRIS Instruments, Orleans, France) and a dipole–dipole skip zero (dipoles with minimal distance equal

to one electrode spacing) acquisition scheme. Time-lapse measurements were taken periodically, using a dipole–dipole skip 0 scheme and full acquisition of reciprocals to estimate the data error level [96,120,121]. Consistently, the data inversion used an Occam inversion approach, as implemented in the Profile R/R2/R3 software package, accounting for the error level estimated from the data themselves [114]. Results are shown in Figures 9–11.

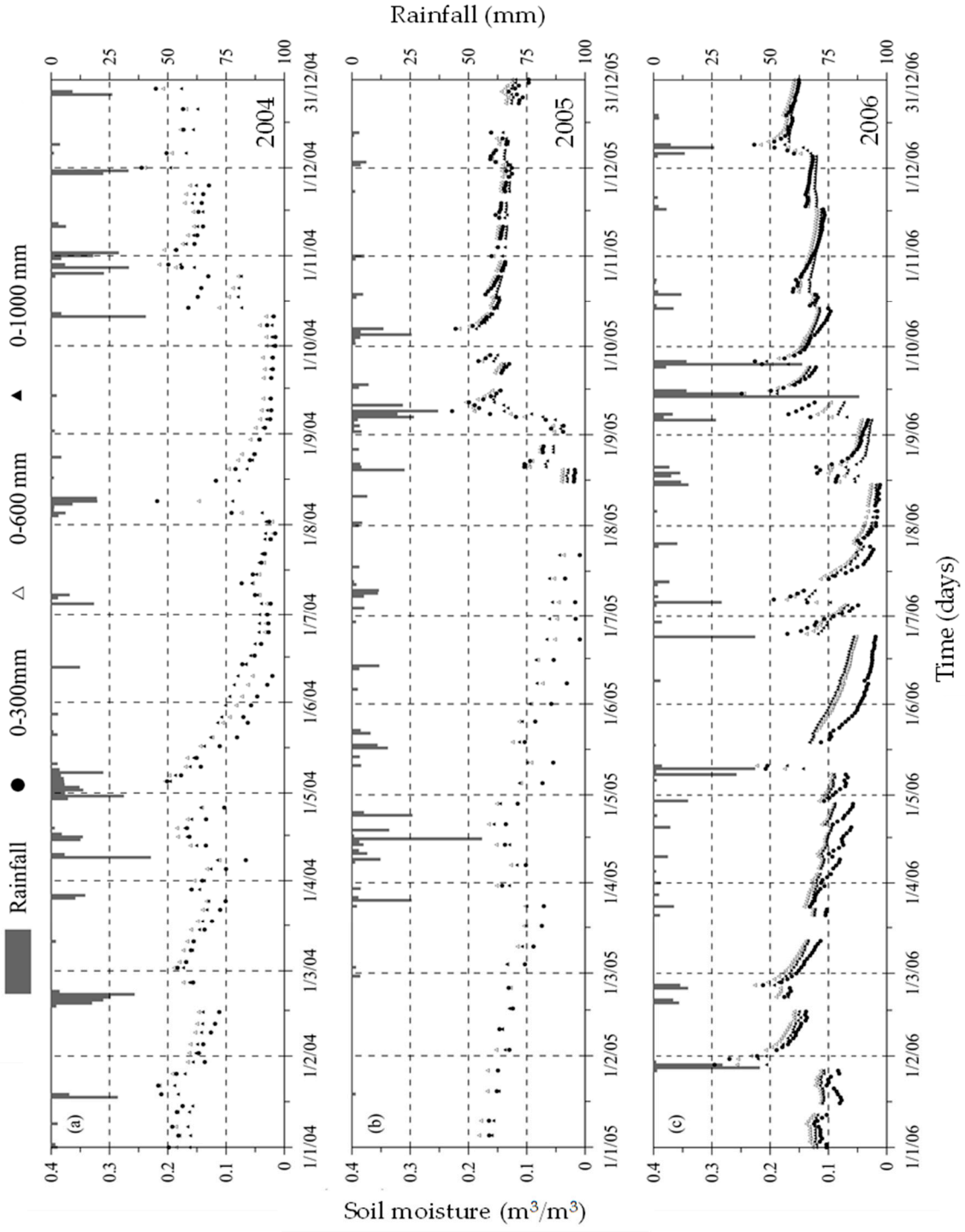

Figure 7. Grugliasco site, 2004–2006. Daily soil water content and rainfall data within the layers 0–0.3, 0–0.6, and 0–1.0 m from 1 January 2004 to 31 December 2006. Since 2005 data have been automatically sampled at hourly step intervals.

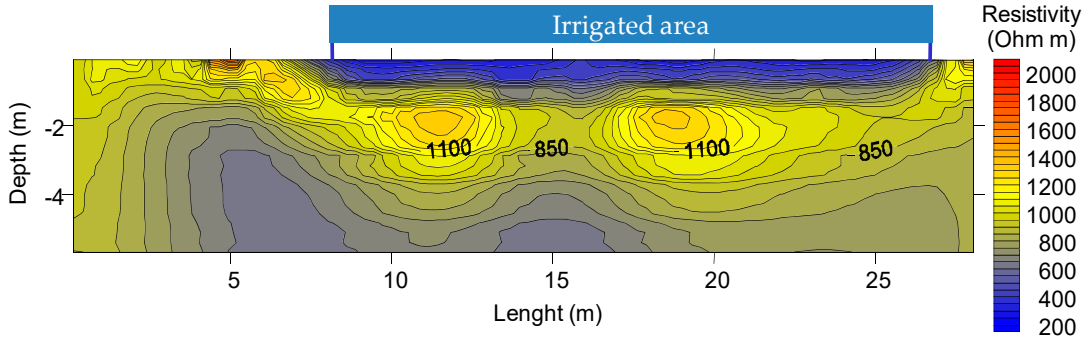

Figure 8. Grugliasco site, 28 August 2009 (hour 17:30). Absolute ERT image at the end of irrigation along the longitudinal ERT line (see Figure 3 for location).

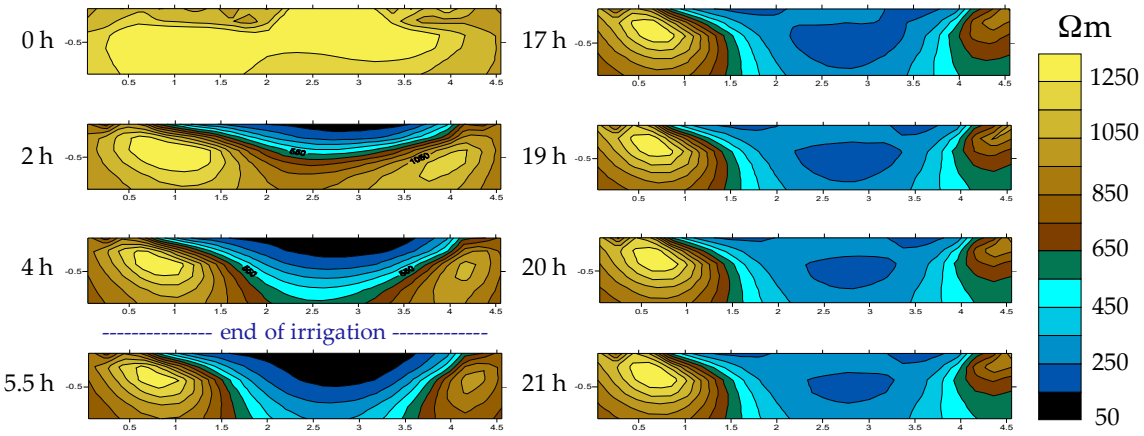

Figure 9. Grugliasco site, August 2009. Absolute ERT images along the transverse line (see Figure 3 for location).

Figure 9 shows the time evolution of absolute resistivity during and after irrigation. The changes in resistivity are particularly clear as the soil profile was initially very dry (at the end of August). The same patterns are apparent, with a more distinctive character, in the relative time-lapse images shown in Figure 10. Here a comparison is also made between a simple approach, where ratios of the absolute images in Figure 9 are taken pixel by pixel, and the more accurate approach based upon ratio inversion, e.g., [96]. In this specific case the two approaches yield practically the same results as, given the geometry of the system and the corresponding resistivity variations over time (the ERT line is transverse to a long stripe where resistivity changes in a fairly homogeneous manner), no 3D effect is present. Note that in general a simple pixel-by-pixel ratio of absolute images does not lead to acceptable results, as the absolute images are 2D inversions in what is actually a 3D space, and ratio or difference inversions shall be used [122].

Finally, Figure 11 shows the estimated soil moisture patterns in the ERT section, derived from converting resistivity into moisture content by means of a laboratory-calibrated Archie's law [86]. The infiltration front estimated by GPR measurements is also depicted (red dotted lines).

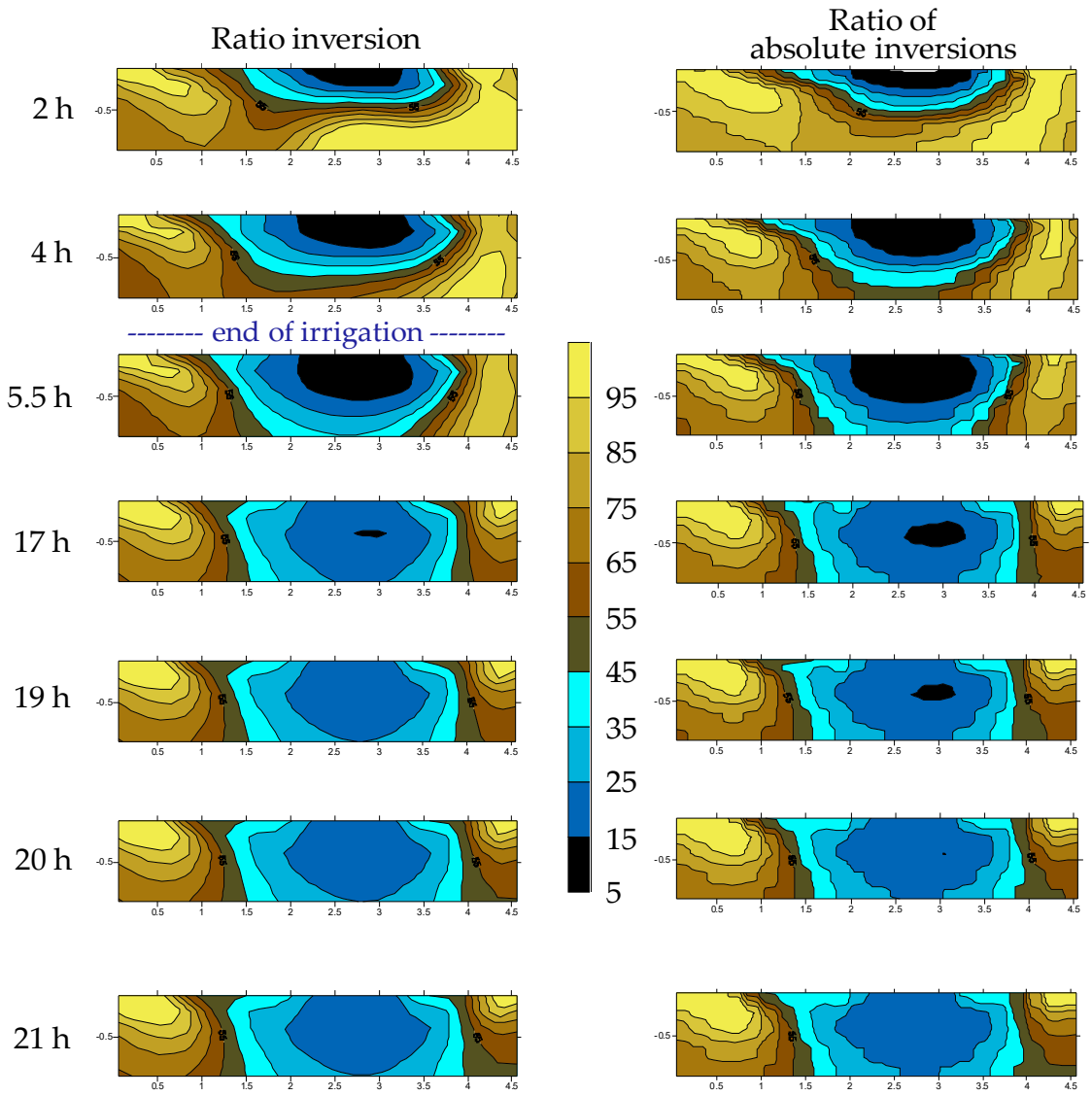

Figure 10. Grugliasco site, August 2009. Relative ERT images along the transverse line (see Figure 3 for location). Both results of ratio inversion and ratios of absolute inversion are shown as percentage of the background (pre-irrigation) values. In this case the two approaches yield very similar results, as the resistivity changes occur homogeneously across the measurement line (no 3D effects).

The performed TDR measurements are depicted in Figure 12 as a function of time and depth. The data are represented as averaged values together with their standard deviations. Initial conditions are dry and homogeneous with soil water contents about 0.08–0.10 m^3/m^3 along all the investigated soil profiles. After the first irrigation step the surface layer immediately reaches values close to saturation (about 0.30 m^3/m^3), but variability is evident between measurements despite the uniform testing conditions. In the following irrigation steps the saturation conditions persist in the surface layer investigated but the variability between measurements progressively decreases. Considering the whole profile, the soil moisture gradually increases along with the irrigation volumes. The following day, starting with the early morning, conditions changed considerably. At the surface, the soil moisture was more uniform and decreased from saturation conditions down to the field capacity (around 0.17 m^3/m^3), while, considering the whole depth investigated, conditions remain the same. All these considerations agree and integrate the information provided by the ERT imaging.

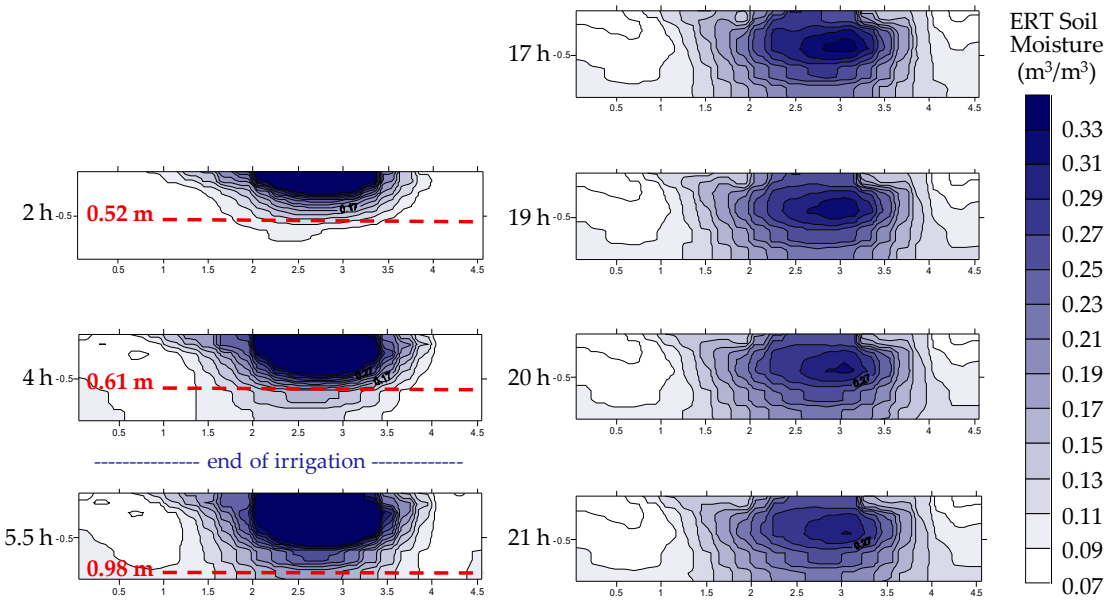

Figure 11. Grugliasco site, August 2009. Moisture content at different times after irrigation, estimated from ERT imaging and laboratory calibrated Archie's law results. A comparison is made against the depth of the infiltration front estimated by GPR measurements (red dotted lines) [32].

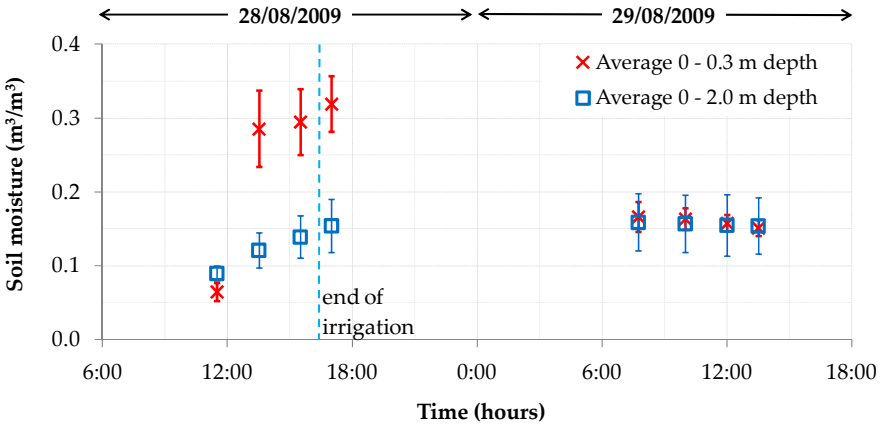

Figure 12. Grugliasco site, August 2009. Moisture contents and their standard deviation at different times after irrigation, computed from TDR measurements.

Usability of TDR for deep soil measurement campaigns. A further interesting application for a low-attenuation porous medium (such as the Grugliasco sandy soil case) is represented by the suitability of TDR technique to investigate very thick layers (down to 4 m). Despite the complications connected with the probes' insertion (where an insertion guide apparatus is essential to prevent geometrical probe deformations), Figure 13 illustrates the waveform detected during a single measurement campaign with soil moisture ranging between 0.11 and 0.14 m^3/m^3 along the profile. Only the surface layer (0–0.5 m depth) shows a higher value, around 0.22 m^3/m^3. Figure 13 highlights that retrieved waveforms are really clear, even for 4 m long probes, and signal reflections are evident and easy toanalyse.

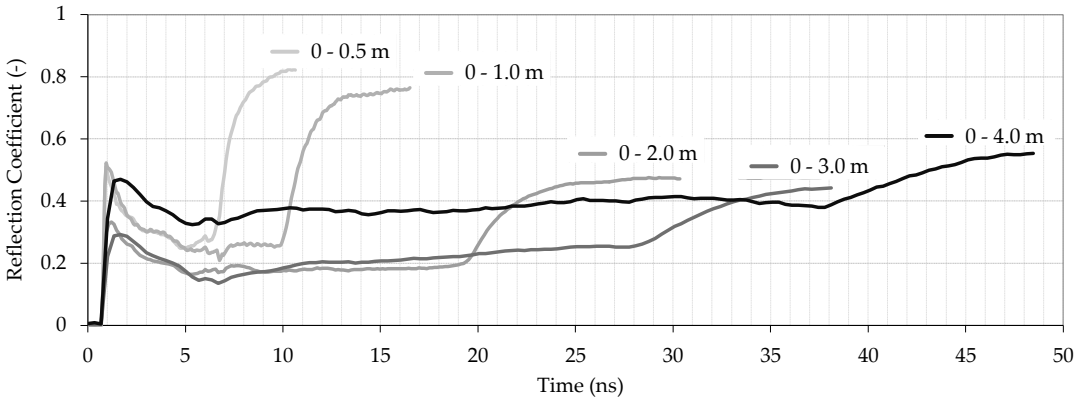

Figure 13. Grugliasco site, 20 May 2010. Waveforms detected with different TDR waveguides lengths vertically inserted into the soil from the surface down to 4 m depth.

4.2. Mountain Permanent Meadow

Long-term soil moisture measurements. In the graph below (Figure 14), the soil volumetric water content—averaged every 30 min—together with rainfall data—collected by the ARPA VdA meteorological station located nearby—are plotted on an hourly base from 1 January to 31 December 2016.

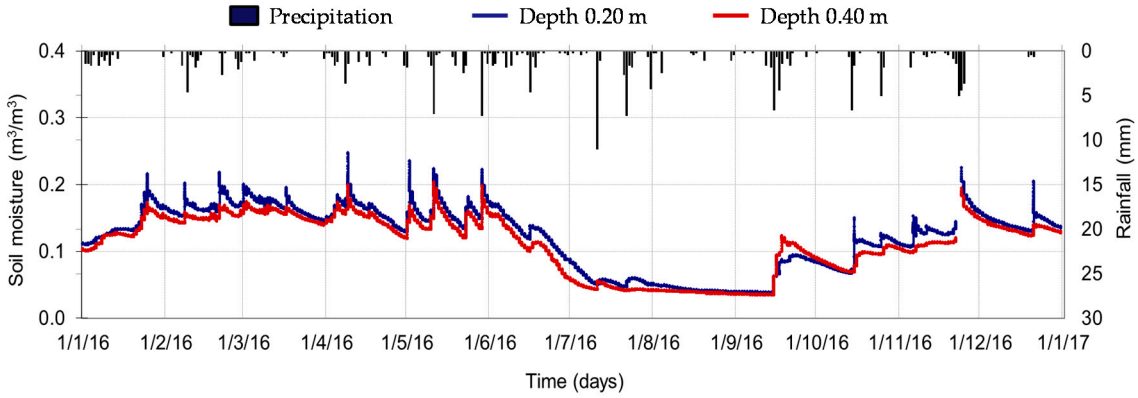

Figure 14. Cogne site, January–December 2016. Precipitation and soil moisture measured at 0.20 and 0.40 m depths.

The volumetric soil moisture collected in the Gimillan site (Figure 4) during the whole year 2016 never exceeded 0.3 m^3/m^3. This threshold can be considered to be in agreement with the literature data for coarse texture soils. Interesting data can be observed at the beginning of the year. In this period the soil is frozen, with a low amount of liquid water content. Then, in the second half of January, a peak occurs without any surveyed rainfall. This behaviour can be ascribed to the soil water (and snow) melting due to the temperature increase, especially considering the south–southeast aspect. Other interesting data can be provided during the summer (in particular from July to the first half of September). In this period, soil moisture is characterized by progressively lower values, with a minimum situated around 0.05 m^3/m^3. In this dry period the correspondence between the occurrence of rainfalls and soil moisture increase is not so evident. This behaviour might be attributed to the effect of the dense vegetation coverage (withered by the water scarcity), driving to interception rather than infiltration into the soil.

With reference to the soil moisture dynamics, fast-acting peaks of soil water increase/decrease can be observed. This attitude can mainly be attributed to the following factors: (1) hydrological properties of the coarse soil texture (e.g., fast infiltration processes; limited water retention/storage);

(2) morphological characteristics of the site, namely the SSE slope aspect, which implies accelerated atmospheric and evaporation dynamics (e.g., solar radiation incidence; mountain/valley breezes). Notwithstanding the abovementioned aspects, it is interesting to highlight that during the surveyed period, the soil moisture values detected at 0.20 m depth were higher than the 0.40 m depth ones, probably due to the dense vegetation and the spatial variability. However, the time dynamic is more enhanced at 20 cm depth.

EMI, ERT and TDR measurement campaigns. EMI surveys at this site are particularly complex given the steep slope and the shrubs (see Figure 4), thus spatial sampling is different at the two dates (as seen in the extent of the mapped areas represented in Figure 15). The most evident feature refers to the strong difference in mean electrical resistivity, with October being much drier than September. Here, the irregular morphology characterized by depressions and bumps, together with the variability of soil and soil-cover vegetation, led to heterogeneous dynamics in time and space, more evident in drier conditions.

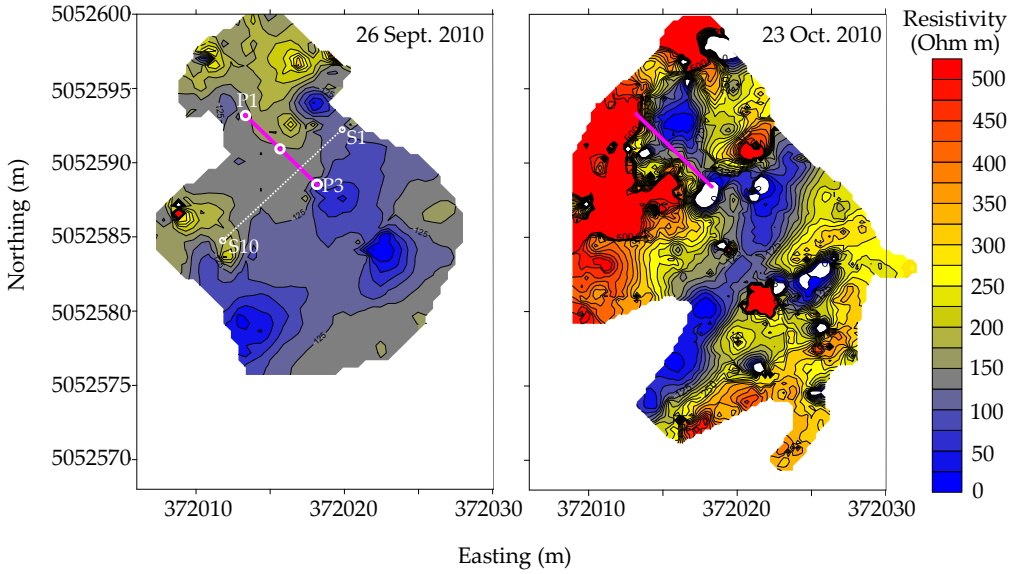

Figure 15. Cogne site, 2010. EMI maps, shown as electrical resistivity values. The strong change between 26 September (more conductive) and 23 ctober (more resistive) is remarkable. The maps represent the mean electrical resistivity from the ground surface to a depth estimated around 1.5 m. The purple line shows the location of the ERT line (results in Figure 16). The white dots represent the two TDR transects: P indicates the progressive 0.75 m depth measurements; S indicates the progressive 0.15 and 0.30 m depth measurements.

It is very informative to compare EMI maps with localized ERT profiles (Figure 16). The latter are taken in reference to the purple line marked in Figure 13. Considering that the values in the EMI maps are obtained in a configuration that gives one value somehow averaged from the ground surface down to 1.5 m depth, i.e., practically involving the entire thickness shown by ERT sections in Figure 16, and given the strong resistivity contrast (both in September and October), this average only has an indicative meaning. Exploring the ERT transects output, note how at both times the shallow soil layer (around 0.5 m thick) is much more resistive than the deeper subsoil. This leads to a very heterogeneous soil profile, so that the EMI maps in Figure 15 only provide a rough mean of the electrical properties averaged over very different values. The ERT images show, consistently with the EMI maps, that in October the site was much drier than in September. More advanced approaches using multi-coil/multi-frequency EMI and depth inversion are, in general, strongly recommended, e.g., [91].

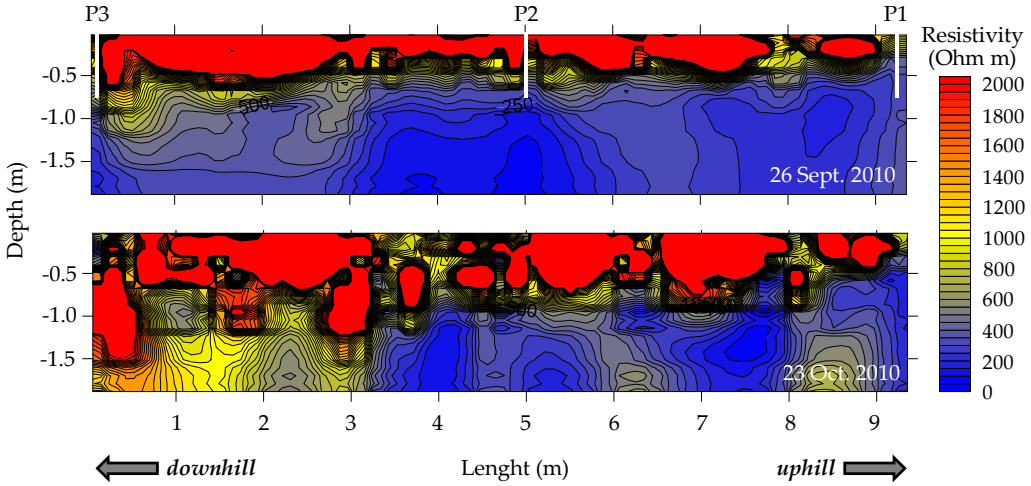

Figure 16. Cogne site, 2010. ERT profiles acquired at the two survey dates along a short profile (see Figure 15 for location). The white lines identified by the P indicate the three 0.75 m depths TDR measurement points. Note that the resistivity scale is much larger in the ERT profiles than in the EMI maps, in order to give a clearer presentation of the variations of resistivity with depth.

Values summarized in Table 2 highlight a general agreement between TDR water content and ERT resistivity behaviour along all the transect ("P" values—see Figure 16 for the exact location). "S" values—see Figure 15 for the transect identification—confirm the water content decrease in the upper layers where the resistivity is higher (as easily seen also in Figure 16) but a strong variability connected with the irregular micro morphology of each measurement point become evident.

Table 2. Cogne site, 2010. TDR soil moisture values measured during the 26 September 2010 EMI and ERT monitoring campaigns. The two TDR transect alignments are depicted in Figure 15.

Probe Code	Transect "P"			Transect "S"														
	P1	*P2*	*P3*	*S1*	*S2*		*S3*	*S4*		*S5*	*S6*		*S7*	*S8*	*S9*		*S10*	
Depth from surface (m)		0.75		0.15	0.15	0.30	0.15	0.15	0.30	0.15	0.15	0.30	0.15	0.15	0.30	0.15	0.15	0.30
Soil moisture (m^3/m^3)	0.41	0.37	0.38	0.33	0.33	0.31	-	0.39	0.22	0.31	0.41	0.40	0.33	0.35	0.34	0.32	0.32	0.27

During the 23 October 2010 EMI and ERT monitoring campaigns, no TDR specific transects were surveyed, however, the CS616 0.10 m depth probe provided the hourly dataset depicted in Figure 15. Despite the data gaps, Figure 17 provides interesting information both on the soil moisture dynamics during the days prior to the measurement, and to the absolute measured soil water content (in agreement with the expected values).

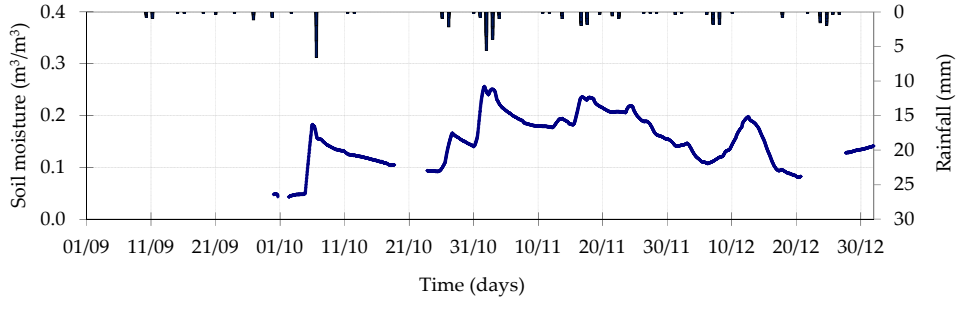

Figure 17. Cogne site, September–December 2010. Precipitation and soil moisture at 0.10 m depth.

4.3. Hilly Vineyard

Long-term soil moisture measurements. A plot of the soil moisture data detected at different depths (namely 0.1, 0.2, 0.3 and 0.4 m below the surface) is depicted in Figure 18, together with the rainfall data.

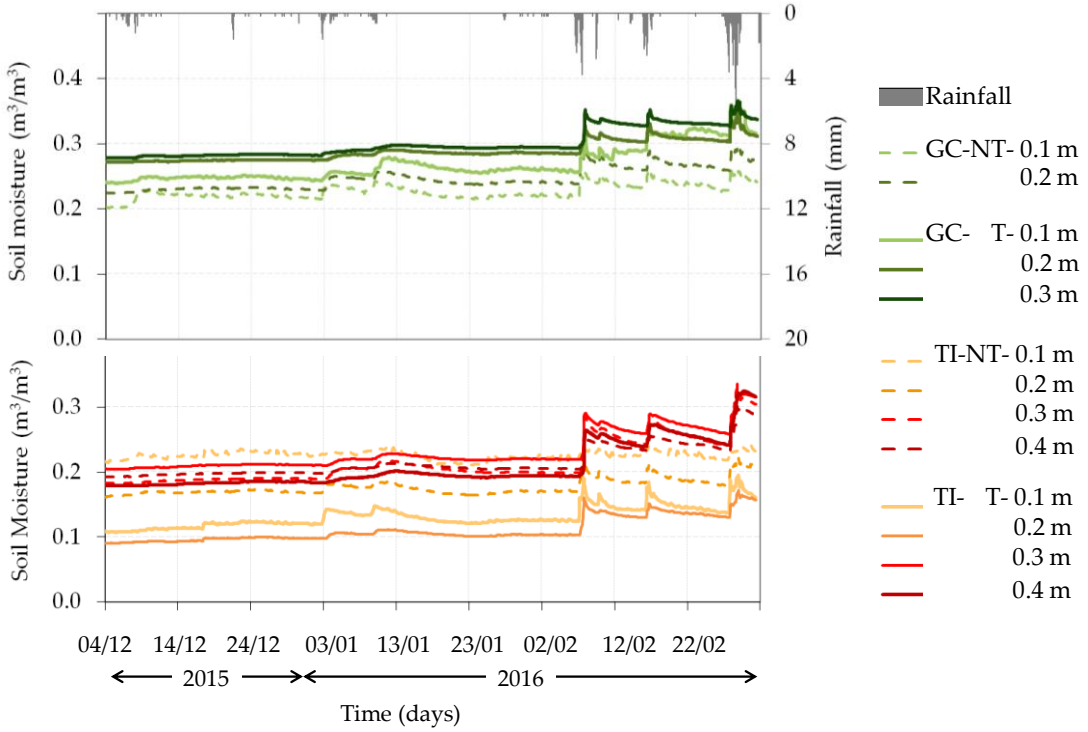

Figure 18. Carpeneto site, winter 2015–2016. Rainfall and soil moisture data collected with an hourly time step (from 0.1 to 0.4 m soil depths). Green lines refer to the Grass Cover condition (GC); red lines refer to the Conventional Tillage condition (TI). Dotted lines refer to the "No Track" condition (NT); solid lines refer to the "Track" condition (T).

The results of the long-term survey (Figure 18) suggest that, under conventional tillage conditions, surface soil moisture in the track position was usually lower than in the central no-track zone. In agreement with Leonard and Andrieux [123] (who found that the major causes in variability of infiltration rates in vineyards are referred to the history of cultivation and the structure of the first soil centimetres), the monitored behaviour can mainly be ascribed to both the agricultural treatment and the soil compaction.

In the grass-covered plot, the soil moisture in the track position was slightly higher than in the central no-track zone along the whole monitoring period. As already observed by Ferrero et al. [124], the tractor traffic in vineyards has a great influence on the spatial variability of soil physical properties, which are strictly related to the topsoil water content. The recurrence of tillage could temporarily decrease this effect, but affects the variability of soil properties over a long period (for more details, see Biddoccu et al. [97]).

EMI and TDR combined campaign. The following Figure 19 show the result obtained the 21 March 2016, from the top of the hill down to the bottom (the last meters of the transects were excluded to avoid measurement distortions due to the presence of a steel grid used to survey the runoff erosion). EMI data were collected in all the rows, starting from the right side (row 18) and moving to the left side (row 0).

In Figure 19, the dots represent the TDR measurement sites along the two transects. The TDR output values are depicted in Figure 20.

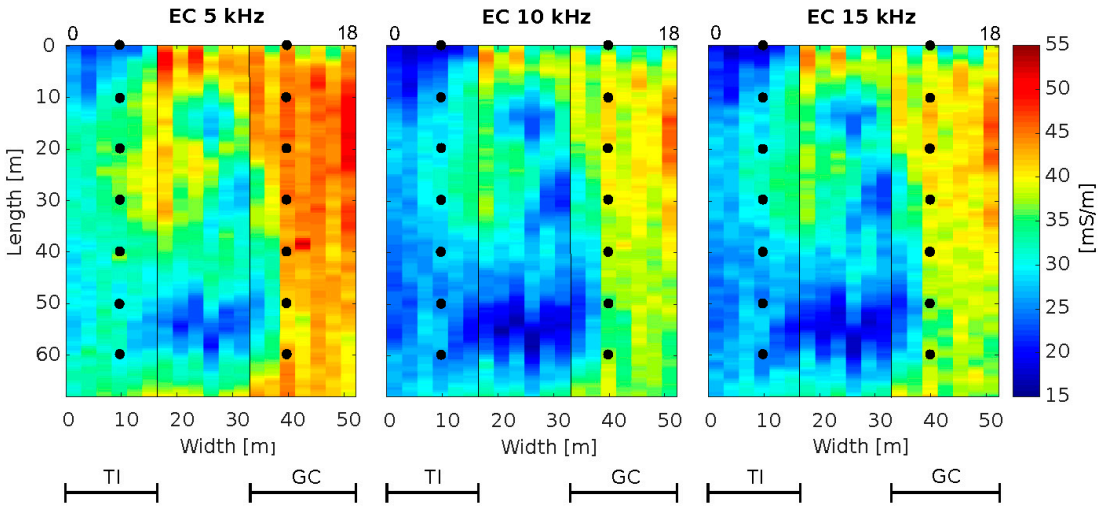

Figure 19. Carpeneto site, 21 March 2016. Electrical conductivity monitored by the EMI equipment and TDR probes locations (black dots) in the testing plot. The three images represent lower depths of investigation, from right to left.

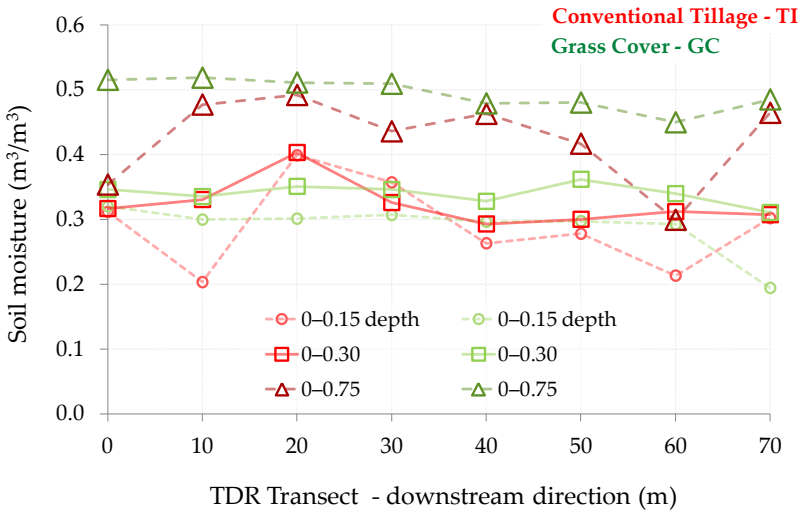

Figure 20. Carpeneto site, 21 March 2016. Soil water content monitored along the two TDR transects (conventional tillage and grass cover) depicted in Figure 19.

The correlation between EC_a and soil moisture is evident (Figures 19 and 20). The results of the EMI measurement campaign show EC_a values along the TI rows lower than those measured along the GC rows. The high value of EC_a along the GC rows can be ascribed to the soil water content, which is higher than in the TI rows, especially in the deeper layers (Figure 20). Moreover, EC_a measured at 5 kHz (highest depth of investigation) is higher than EC_a measured at 10 and 15 kHz, and is in agreement with the soil water content measured by TDR (Figure 20) and also with the long-term measurements (Figure 18). However, the low EC_a values at the bottom of the TI rows (corresponding to the 60 m coordinate) do not completely agree with the TDR water content value: at this point, notwithstanding the lowest TI soil moisture, the EC_a values are not as low as the values detected in similar conditions. Being in the tilled area, this behaviour might be ascribed to the deposition of fine particles eroded from the top toward the bottom.

5. Discussion

Through a comprehensive analysis of the presented case studies, it is possible to evaluate the application pros and cons of the different methods used.

The TDR technique offers wide flexibility in different contexts for both single campaigns and long-term surveys, with excellent temporal and spatial resolution attainable through the automation of measurements. Measurements are rapid, non-destructive and simple to obtain. The higher the number of probes to be acquired simultaneously, the more complex the system will have to be (eventually adopting a multiplexed system). Depending on the monitoring needs, specific experimental layouts can be adopted with vertical and/or horizontal probes of different lengths. In ideal conditions (i.e., low-attenuation porous media with no coarse skeletal material—stones/rocks) TDR probes can be vertically inserted down to unusual depths (e.g., 4 m, as demonstrated in the plain permanent meadow case study) to explore the soil water content/behaviour below the most commonly monitored layers. For these last applications, the adoption of a steel guide during the insertion process is strongly recommended to maintain rods in parallel and prevent geometrical probe deformations. Due to the TDR's inability to detect liquid and ice contents simultaneously (within a bandwidth between a few megahertz and 1.5 GHz), in the case of frozen soils additional measurements with lower frequencies (between 0.1 and 200 kHz [118,119]) would be necessary to avoid underestimations or errors.

Low-frequency sensors directly connected to data loggers combine good accuracy and reliability with a lower cost (and can be used in place of TDR). By their nature they need specific calibration and they suffer from some restrictions related to the constructive features (e.g., probe lengths; more fragility—depending on the types and models), but they are easy to use and efficient in the most common soil moisture investigations.

To determine the spatial distribution of soil moisture, whereas TDR evaluates the specific water content analysing the full signal response (and relating it to the dielectric properties), the ERT system determines the two-dimensional electric resistivity distribution (from surface-based geoelectric measurements and subsequent data inversion). A combination of both methods would lead to better results (e.g., for calibrating the ERT approach). However, determining the soil water content from the resulting electrical resistivity values is more difficult than in the case of the dielectric coefficients using TDR. The inversion procedure can produce mass balance errors, due to a rapid decrease of ERT resolution with depth [40]. This problem may be solved through a coupled hydro-geophysical approach [40,101]. However, if only qualitative assessment of spatial distribution and time variations of soil moisture content are sufficient, an uncoupled approach can be used [32], based on the following steps: (1) inversion of geophysical field data gives the spatial distribution of electrical resistivity; (2) application of a petro-physical relationship to obtain an estimation of moisture content distribution from the electrical resistivity.

It must be noted that electrical resistivity and electrical conductivity, as measured by EMI, are just reciprocal quantities. Thus ERT and EMI measure the same physical parameter, and can be effectively used to complement each other: EMI gives quicker information over large areas, while ERT is more effective at in-depth investigations. In the hilly vineyard test case, for example, EMI measurements allow for identifying differences in EC_a (and thus soil moisture) between the two treatments and in relation to depth, with results that are comparable with the more accurate (and time-consuming) TDR measurements. In the permanent mountain meadow, since EMI measurements are fast (and not invasive), it was possible to map the EC_a spatial variations over the whole field-size plot (also in complex logistical conditions). Some discordances between EMI and TDR measurements could be ascribed to local conditions that can affect TDR local measurements. When possible, a combined EMI and TDR campaign allows us to combine accuracy with wider spatial representativeness of measurements than only TDR campaigns.

Without considering the borehole applications (which have not been analysed in this work), GPR can be used to perform specific campaigns aimed at obtaining soil sub-surface "images" (typically in the range of sub-meters up to tens of meters) referred to the interaction between the transmitted

EM energy and the spatial variation in the complex, frequency-dependent EM properties of the earth materials in the subsurface [125]. For small-scale, site-specific experiments, GPR can be used to monitor the movement of water into the—and through the—subsurface (such as the depth of the infiltration front estimated by GPR measurements in the plain permanent meadow case study). However, the use of GPR systems remains difficult in uneven irregular areas due to the need to drag the instrument to keep it in contact with the soil surface (such as at the permanent mountain meadow testing site). Limitations are also acknowledged in clay-laden soils (such as the hilly vineyard testing site), where the signal penetration into the soil is strongly reduced by the high electrical conductivity.

6. Conclusions

Soil moisture is highly variable at both the spatial and the temporal scale, and soil moisture field measurements are recognized to be fundamental in the integration of in situ, satellite and modelled data. For these reasons, in our work we provide a synoptic view of techniques, supported by case studies, to show that also in very different field conditions (in terms of altitude, land use, and soil type, namely a plain, a mountain meadow and a hilly vineyard) it is possible to estimate time and spatially resolved soil moisture by the same combination of instruments: contact-based methods (i.e., Time Domain Reflectometry—TDR, and two low-frequency probes) for the time resolved, and minimally invasive hydro-geophysical methods (i.e., Electromagnetic Induction—EMI, Ground Penetrating Radar—GPR, and the Electrical Resistivity Tomography—ERT) for the spatially resolved. By doing so, soil moisture dynamics determined by soil's heterogeneity and meteorological events can be efficiently observed and measured. In particular, while plot-scale methods—like EMI, GPR and ERT—provide efficient spatial surveys, local-scale methods—like TDR and other lower-cost soil moisture sensors—provide efficient soil moisture monitoring across time (and space—where properly structured). With less accuracy, and with smaller volume support, the low-frequency sensors can also be used in place of TDR.

An important key future challenge might be represented by the creation of a framework in which the information contained in the local and plot observations is combined with model predictions of soil moisture dynamics, at different spatial scales. Nowadays, this integrated approach would represent the best method to achieve the great potential, especially in hydrological applications, of soil moisture studies.

Acknowledgments: This work has been partially funded by the EU-funded H2020 Project "*ECOPOTENTIAL: Improving Future Ecosystem Benefits through Earth Observations*" (http://www.ecopotential-project.eu) and the Italian National Research Programme 2011–2013 by The Project of Interest "*NextData: a national system for the retrieval, storage, access and diffusion of environmental and climate data from mountain and marine areas*" (http://www.nextdataproject.it/?q=en). The "Agrion—Centro sperimentale per la Vitivinicoltura" (which managed the "Tenuta Cannona" vineyards), is also gratefully acknowledged.

Author Contributions: All co-authors, each within his competence, actively participated in the field campaigns, data processing, and data analysis. Stefano Ferraris is the Grugliasco and Cogne experimental sites scientific coordinator. Eugenio Cavallo coordinated the experiments in Tenuta Cannona. Giulia Raffelli, Stefano Ferraris and Maurizio Previati conceived and designed the paper. The manuscript was written by Maurizio Previati, Giulia Raffelli, Davide Canone, Stefano Ferraris and Giorgio Cassiani. Maurizio Previati, Ivan Bevilacqua, Giulia Raffelli, Giorgio Cassiani and Stefano Ferraris contributed to the figures and the manuscript editing.

Conflicts of Interest: The authors declare no conflict of interest.

References

1. Lin, H. Temporal stability of soil moisture spatial pattern and subsurface preferential flow pathways in the shale hills catchment. *Vadose Zone J.* **2006**, *5*, 317–340. [CrossRef]
2. Tromp-van Meerveld, H.J.; McDonnell, J.J. On the interrelations between topography, soil depth, soil moisture, transpiration rates and species distribution at the hillslope scale. *Adv. Water Resour.* **2006**, *29*, 293–310. [CrossRef]

3. Teuling, A.J.; Hupet, F.; Uijlenhoet, R.; Troch, P.A. Climate variability effects on spatial soil moisture dynamics. *Geophys. Res. Lett.* **2007**, *34*. [CrossRef]
4. Vereecken, H.; Huisman, J.A.; Bogena, H.; Vanderborght, J.; Vrugt, J.A.; Hopmans, J.W. On the value of soil moisture measurements in vadose zone hydrology: A review. *Water Resour. Res.* **2008**, *44*. [CrossRef]
5. Vereecken, H.; Huisman, J.A.; Pachepsky, Y.; Montzka, C.; Van Der Kruk, J.; Bogena, H.; Vanderborght, J. On the spatio-temporal dynamics of soil moisture at the field scale. *J. Hydrol.* **2014**, *516*, 76–96. [CrossRef]
6. Ceaglio, E.; Mitterer, C.; Maggioni, M.; Ferraris, S.; Segor, V.; Freppaz, M. The role of soil volumetric liquid water content during snow gliding processes. *Cold Reg. Sci. Technol.* **2017**, *136*, 17–29. [CrossRef]
7. Bomblies, A. Modeling the role of rainfall patterns in seasonal malaria transmission. *Clim. Chang.* **2012**, *112*, 673–685. [CrossRef]
8. Previati, M.; Bevilacqua, I.; Canone, D.; Ferraris, S.; Haverkamp, R. Evaluation of soil water storage efficiency for rainfall harvesting on hillslope micro-basins built using time domain reflectometry measurements. *Agric. Water Manag.* **2010**, *97*, 449–456. [CrossRef]
9. Canone, D.; Previati, M.; Bevilacqua, I.; Salvai, L.; Ferraris, S. Field measurements based model for surface irrigation efficiency assessment. *Agric. Water Manag.* **2015**, *156*, 30–42. [CrossRef]
10. Canone, D.; Previati, M.; Ferraris, S. Evaluation of Stemflow Effects on the Spatial Distribution of Soil Moisture Using TDR Monitoring and an Infiltration Model. *J. Irrig. Drain. Eng. ASCE* **2017**, *143*, 04016075. [CrossRef]
11. Robinson, D.A.; Campbell, C.S.; Hopmans, J.W.; Hornbuckle, B.K.; Jones, S.B.; Knight, R.; Ogden, F.; Selker, J.; Wendroth, O. Soil moisture measurement for ecological and hydrological watershed-scale observatories: A review. *Vadose Zone J.* **2008**, *7*, 358–389. [CrossRef]
12. Fares, A.; Temimi, M.; Morgan, K.; Kelleners, T.J. In-situ and remote soil moisture sensing technologies for vadose zone hydrology. *Vadose Zone J.* **2013**, *12*. [CrossRef]
13. Brocca, L.; Ciabatta, L.; Massari, C.; Camici, S.; Tarpanelli, A. Soil Moisture for Hydrological Applications: Open Questions and New Opportunities. *Water* **2017**, *9*, 140. [CrossRef]
14. Romano, N. Soil moisture at local scale: Measurements and simulations. *J. Hydrol.* **2014**, *516*, 6–20. [CrossRef]
15. Topp, G.C.; Davis, J.L.; Annan, A.P. Electromagnetic determination of soil water content: Measurements in coaxial transmission lines. *Water Resour. Res.* **1980**, *16*, 574–582. [CrossRef]
16. Topp, G.C. State of the art of measuring soil water content. *Hydrol. Process.* **2003**, *17*, 2993–2996. [CrossRef]
17. Robinson, D.A.; Jones, S.B.; Wraith, J.M.; Or, D.; Friedman, S.P. A review of advances in dielectric and electrical conductivity measurement in soils using time domain reflectometry. *Vadose Zone J.* **2003**, *2*, 444–475. [CrossRef]
18. Robinson, D.A.; Jones, S.B.; Blonquist, J.M.; Friedman, S.P. A physically derived water content/permittivity calibration model for coarse-textured, layered soils. *Soil Sci. Soc. Am. J.* **2005**, *69*, 1372–1378. [CrossRef]
19. Kizito, F.; Campbell, C.S.; Campbell, G.S.; Cobos, D.R.; Teare, B.L.; Carter, B.; Hopmans, J.W. Frequency, electrical conductivity and temperature analysis of a low-cost capacitance soil moisture sensor. *J. Hydrol.* **2008**, *352*, 367–378. [CrossRef]
20. Blonquist, J.M.; Jones, S.B.; Robinson, D.A.; Rasmussen, V.P.; Or, D. Standardizing characterization of electromagnetic water content sensors. *Vadose Zone J.* **2005**, *4*, 1048–1058. [CrossRef]
21. Bogena, H.R.; Huisman, J.A.; Oberdorster, C.; Vereecken, H. Evaluation of a low-cost soil water content sensor for wireless network applications. *J. Hydrol.* **2007**, *344*, 32–42. [CrossRef]
22. Rosenbaum, U.; Huisman, J.A.; Weuthen, A.; Vereecken, H.; Bogena, H.R. Sensor-to-sensor variability of the ECH$_2$O EC-5, TE, and 5TE sensors in dielectric liquids. *Vadose Zone J.* **2010**, *9*, 181–186. [CrossRef]
23. Baker, J.M.; Allmaras, R.R. System for automating and multiplexing soil moisture measurement by time-domain reflectometry. *Soil. Sci. Soc. Am. J.* **1990**, *54*, 1–6. [CrossRef]
24. Heimovaara, T.J.; Bouten, W. A computer-controlled 36-channel time domain reflectometry system for monitoring soil water contents. *Water Resour. Res.* **1990**, *26*, 2311–2316.
25. Dobriyal, P.; Qureshi, A.; Badola, R.; Hussain, S.A. A review of the methods available for estimating soil moisture and its implications for water resource management. *J. Hydrol.* **2012**, *458*, 110–117. [CrossRef]
26. Huisman, J.A.; Hubbard, S.S.; Redman, J.D.; Annan, A.P. Measuring soil water content with ground penetrating radar. *Vadose Zone J.* **2003**, *2*, 476–491. [CrossRef]
27. Serbin, G.; Or, D. Ground-penetrating radar measurement of crop and surface water content dynamics. *Remote Sens. Environ.* **2005**, *96*, 119–134. [CrossRef]

28. Lambot, S.; Weihermüller, L.; Huisman, J.A.; Vereecken, H.; Vanclooster, M.; Slob, E.C. Analysis of air-launched ground-penetrating radar techniques to measure the soil surface water content. *Water Resour. Res.* **2006**, *42*. [CrossRef]
29. Lambot, S.; Slob, E.; Chavarro, D.; Lubczynski, M.; Vereecken, H. Measuring soil surface water content in irrigated areas of southern Tunisia using full-waveform inversion of proximal GPR data. *Near Sur. Geophys.* **2008**, *6*, 403–410. [CrossRef]
30. Busch, S.; Van der Kruk, J.; Bikowski, J.; Vereecken, H. Quantitative conductivity and permittivity estimation using full-waveform inversion of onground GPR data. *Geophysics* **2012**, *77*, H79–H91. [CrossRef]
31. Klotzsche, A.; Van der Kruk, J.; Linde, N.; Doetsch, J.; Vereecken, H. 3-D characterization of high-permeability zones in a gravel aquifer using 2-D crosshole GPR full-waveform inversion and waveguide detection. *Geophys. J. Int.* **2013**, *195*, 932–944. [CrossRef]
32. Rossi, M.; Manoli, G.; Pasetto, D.; Deiana, R.; Ferraris, S.; Strobbia, C.; Cassiani, G. Coupled inverse modeling of a controlled irrigation experiment using multiple hydro-geophysical data. *Adv. Water Resour.* **2015**, *82*, 150–165. [CrossRef]
33. Corwin, D.L.; Lesch, S.M. Apparent soil electrical conductivity measurements in agriculture. *Comput. Electron. Agric.* **2005**, *46*, 11–43. [CrossRef]
34. Robinson, D.A.; Lebron, I.; Kocar, B.; Phan, K.; Sampson, M.; Crook, N.; Fendorf, S. Time-lapse geophysical imaging of soil moisture dynamics in tropical deltaic soils: An aid to interpreting hydrological and geochemical processes. *Water Resour. Res.* **2009**, *45*. [CrossRef]
35. Cassiani, G.; Ursino, N.; Deiana, R.; Vignoli, G.; Boaga, J.; Rossi, M.; Ludwig, R. Non-invasive monitoring of soil static characteristics and dynamic states: A case study highlighting vegetation effects on agricultural land. *Vadose Zone J.* **2012**, *11*. [CrossRef]
36. Brovelli, A.; Cassiani, G. Effective permittivity of porous media: A critical analysis of the complex refractive index model. *Geophys. Prospect.* **2008**, *56*, 715–727. [CrossRef]
37. Brovelli, A.; Cassiani, G. Combined estimation of effective electrical conductivity and permittivity for soil monitoring. *Water Resour. Res.* **2011**, *47*. [CrossRef]
38. Loke, M.H.; Chambers, J.E.; Rucker, D.F.; Kuras, O.; Wilkinson, P.B. Recent developments in the direct-current geoelectrical imaging method. *J. Appl. Geophys.* **2013**, *95*, 135–156. [CrossRef]
39. Vanderborght, J.; Huisman, J.A.; Van der Kruk, J.; Vereecken, H. Geophysical methods for field-scale imaging of root zone properties and processes. In *Soil–Water–Root Processes: Advances in Tomography and Imaging*; Anderson, S.H., Hopmans, J.W., Eds.; SSSA: Madison, WI, USA, 2013; pp. 247–281.
40. Manoli, G.; Rossi, M.; Pasetto, D.; Deiana, R.; Ferraris, S.; Cassiani, G.; Putti, M. An iterative particle filter approach for coupled hydro-geophysical inversion of a controlled infiltration experiment. *J. Comput. Phys.* **2015**, *283*, 37–51. [CrossRef]
41. Hornbuckle, B.K.; England, A.W.; De Roo, R.D.; Fischman, M.A.; Boprie, D.L. Vegetation canopy anisotropy at 1.4 GHz. *IEEE Trans. Geosci. Remote Sens.* **2003**, *41*, 2211–2223. [CrossRef]
42. Saleh, K.; Wigneron, J.P.; Waldteufel, P.; De Rosnay, P.; Schwank, M.; Calvet, J.C.; Kerr, Y.H. Estimates of surface soil moisture under grass covers using L-band radiometry. *Remote Sens. Environ.* **2007**, *109*, 42–53. [CrossRef]
43. Hong, S.; Shin, I. A physically-based inversion algorithm for retrieving soil moisture in passive microwave remote sensing. *J. Hydrol.* **2011**, *405*, 24–30. [CrossRef]
44. Kornelsen, K.C.; Coulibaly, P. Advances in soil moisture retrieval from synthetic aperture radar and hydrological applications. *J. Hydrol.* **2013**, *476*, 460–489. [CrossRef]
45. Reigber, A.; Scheiber, R.; Jager, M.; Prats-Iraola, P.; Hajnsek, I.; Jagdhuber, T.; Horn, R. Very-high-resolution airborne synthetic aperture radar imaging: Signal processing and applications. *Proc. IEEE* **2013**, *101*, 759–783. [CrossRef]
46. Zreda, M.; Desilets, D.; Ferré, T.P.A.; Scott, R.L. Measuring soil moisture content non-invasively at intermediate spatial scale using cosmic-ray neutrons. *Geophys. Res. Lett.* **2008**, *35*. [CrossRef]
47. Zreda, M.; Shuttleworth, W.J.; Zeng, X.; Zweck, C.; Desilets, D.; Franz, T.; Rosolem, R. COSMOS: The COsmic-ray soil moisture observing system. *Hydrol. Earth Syst. Sci.* **2012**, *16*, 4079–4099. [CrossRef]
48. Rivera Villarreyes, C.A.; Baroni, G.; Oswald, S.E. Integral quantification of seasonal soil moisture changes in farmland by cosmic-ray neutrons. *Hydrol. Earth Syst. Sci.* **2011**. [CrossRef]

49. Bogena, H.R.; Huisman, J.A.; Baatz, R.; Hendricks Franssen, H.J.; Vereecken, H. Accuracy of the cosmic-ray soil water content probe in humid forest ecosystems: The worst case scenario. *Water Resour. Res.* **2013**, *49*, 5778–5791. [CrossRef]
50. Zhu, Z.; Tan, L.; Gao, S.; Jiao, Q. Observation on soil moisture of irrigation cropland by cosmic-ray probe. *IEEE Geosci. Remote Sens. Lett.* **2015**, *12*, 472–476. [CrossRef]
51. Shin, Y.; Mohanty, B.P. Development of a deterministic downscaling algorithm for remote sensing soil moisture footprint using soil and vegetation classifications. *Water Resour. Res.* **2013**, *49*, 6208–6228. [CrossRef]
52. Ines, A.V.M.; Mohanty, B.P.; Shin, Y. An unmixing algorithm for remotely sensed soil moisture. *Water Resour. Res.* **2013**, *49*, 408–425. [CrossRef]
53. Peng, J.; Loew, A.; Zhang, S.; Wang, J.; Niesel, J. Spatial downscaling of satellite soil moisture data using vegetation temperature condition index. *IEEE Trans. Geosci. Remote Sens.* **2016**, *54*, 558–566. [CrossRef]
54. Peng, J.; Niesel, J.; Loew, A. Evaluation of soil moisture downscaling using a simple thermal-based proxy: The REMDHUS network (Spain) example. *Hydrol. Earth Syst. Sci.* **2015**, *19*, 4765–4782. [CrossRef]
55. Calvet, J.-C.; Noilhan, J. From near-surface to root-zone soil moisture using year-round data. *J. Hydrometeorol.* **2000**, *1*, 393–411. [CrossRef]
56. Sabater, J.M.; Jarlan, L.; Calvet, J.C.; Bouyssel, F.; De Rosnay, P. From near-surface to root-zone soil moisture using different assimilation techniques. *J. Hydrometeorol.* **2007**, *8*, 194–206. [CrossRef]
57. Albergel, C.; Rudiger, C.; Pellarin, T.; Calvet, J.-C.; Fritz, N.; Froissard, F.; Suquia, D.; Petitpa, A.; Piguet, B.; Martin, E. From near-surface to root-zone soil moisture using an exponential filter: An assessment of the method based on in-situ observations and model simulations. *Hydrol. Earth Syst. Sci.* **2008**, *12*, 1323–1337. [CrossRef]
58. Manfreda, S.; Brocca, L.; Moramarco, T.; Melone, F.; Sheffield, J. A physically based approach for the estimation of root-zone soil moisture from surface measurements. *Hydrol. Earth Syst. Sci.* **2014**, *18*, 1199–1212. [CrossRef]
59. Tebbs, E.; Gerard, F.; Petrie, A.; DeWitte, E. Emerging and Potential Future Applications of satellite-Based Soil Moisture products. In *Satellite Soil Moisture Retrievals: Techniques and Applications*; Petropoulos, G.P., Srivastava, P., Kerr, Y., Eds.; Elsevier: Amsterdam, The Netherlands, 2016; Volume 19, pp. 379–400.
60. Peng, J.; Loew, A.; Merlin, O.; Verhoest, N.E.C. A review of spatial downscaling of satellite remotely sensed soil moisture. *Rev. Geophys.* **2017**, *55*, 341–366. [CrossRef]
61. Mohanty, B.P.; Cosh, M.H.; Lakshmi, V.; Montzka, C. Soil moisture remote sensing: State-of-the-science. *Vadose Zone J.* **2017**, *16*. [CrossRef]
62. Desilets, D.; Zreda, M. Footprint diameter for a cosmic-ray soil moisture probe: Theory and Monte Carlo simulations. *Water Resour. Res.* **2013**, *49*. [CrossRef]
63. Franz, T.E.; Zreda, M.; Ferré, T.P.A.; Rosolem, R.; Zweck, C.; Stillman, S.; Zeng, X.; Shuttleworth, W.J. Measurement depth of the cosmic ray soil moisture probe affected by hydrogen from various sources. *Water Resour. Res.* **2012**, *48*, W08515. [CrossRef]
64. Köhli, M.; Schrön, M.; Zreda, M.; Schmidt, U.; Dietrich, P.; Zacharias, S. Footprint characteristics revised for field-scale soil moisture monitoring with cosmic-ray neutrons. *Water Resour. Res.* **2015**, *51*, 5772–5790. [CrossRef]
65. Hallikainen, M.T.; Ulaby, F.T.; Dobson, M.C.; El-Rayes, M.A.; Wu, L.K. Microwave dielectric behavior of wet soil-part 1: Empirical models and experimental observations. *IEEE Trans. Geosci. Remote Sens.* **1985**, *1*, 25–34. [CrossRef]
66. Evett, S.R. Soil water measurement by time domain reflectometry. In *Encyclopedia of Water Science*; United States Department of Agriculture (USDA): Bushland, TX, USA, 2003; pp. 894–898.
67. Topp, G.C.; Ferré, T.P.A. Methods for measurement of soil water content: Time domain reflectometry. In *Methods of Soil Analysis, Part 4*; Dane, J.H., Topp, G.C., Eds.; SSSA Book Series No. 5; Soil Science Society of America: Madison, WI, USA, 2002; pp. 434–446.
68. Roth, K.; Schulin, R.; Flühler, H.; Attinger, W. Calibration of time domain reflectometry for water content measurement using a composite dielectric approach. *Water Resour. Res.* **1990**, *26*, 2267–2273. [CrossRef]
69. Herkelrath, W.N.; Hamburg, S.P.; Murphy, F. Automatic, real-time monitoring of soil moisture in a remote field area with time domain reflectometry. *Water Resour. Res.* **1991**, *27*, 857–864. [CrossRef]
70. Topp, G.C.; Davis, J.L.; Annan, A.P. Electromagnetic determination of soil water content using TDR: I. Applications to wetting fronts and steep gradients. *Soil Sci. Soc. Am. J.* **1982**, *46*, 672–678. [CrossRef]

71. Topp, G.C.; Davis, J.L.; Annan, A.P. Electromagnetic determination of soil water content using TDR: II. Evaluation of installation and configuration of parallel transmission lines. *Soil Sci. Soc. Am. J.* **1982**, *46*, 678–684. [CrossRef]
72. Zegelin, S.J.; White, I.; Jenkins, D.R. Improved field probes for soil water content and electrical conductivity measurement using time domain reflectometry. *Water Resour. Res.* **1989**, *25*, 2367–2376. [CrossRef]
73. Heimovaara, T.J. Design of triple-wire time domain reflectometry probes in practice and theory. *Soil Sci. Soc. Am. J.* **1993**, *57*, 1410–1417. [CrossRef]
74. Ferré, P.A.; Rudolph, D.L.; Kachanoski, R.G. Spatial averaging of water content by time domain reflectometry: Implications for twin rod probes with and without dielectric coatings. *Water Resour. Res.* **1996**, *32*, 271–279. [CrossRef]
75. Ferré, P.A.; Knight, J.H.; Rudolph, D.L.; Kachanoski, R.G. The sample areas of conventional and alternative time domain reflectometry probes. *Water Resour. Res.* **1998**, *34*, 2971–2979. [CrossRef]
76. Canone, D.; Previati, M.; Ferraris, S.; Haverkamp, R. A new coaxial time domain reflectometry probe for water content measurement in forest floor litter. *Vadose Zone J.* **2009**, *8*, 363–372. [CrossRef]
77. Adelakun, I.A.; Ranjan, R.S. Design of a Multilevel TDR Probe for Measuring Soil Water Content at Different Depths. *Trans. ASABE* **2013**, *56*, 1451–1460. [CrossRef]
78. Nissen, H.H.; Ferré, T.P.A.; Moldrup, P. Sample area of two- and three-rod time domain reflectometry probes. *Water Resour. Res.* **2003**, *39*, 1289. [CrossRef]
79. Vaz, C.M.; Jones, S.; Meding, M.; Tuller, M. Evaluation of standard calibration functions for eight electromagnetic soil moisture sensors. *Vadose Zone J.* **2013**, *12*. [CrossRef]
80. Campbell, C.S.; Campbell, G.S.; Cobos, D.R.; Bissey, L.L. Calibration and Evaluation of an Improved Low-Cost Soil Moisture Sensor. 2009. Available online: http://www.decagon.com (accessed on 12 September 2017).
81. Logsdon, S.D.; Hernandez-Ramirez, G.; Hatfield, J.L.; Sauer, T.J.; Prueger, J.H.; Schilling, K.E. Soil water and shallow groundwater relations in an agricultural hillslope. *Soil Sci. Soc. Am. J.* **2009**, *73*, 1461. [CrossRef]
82. Parsons, L.R.; Bandaranayake, W.M. Performance of a new capacitance soil moisture probe in a sandy soil. *Soil Sci. Soc. Am. J.* **2009**, *73*, 1378–1385. [CrossRef]
83. Evett, S.R.; Schwartz, R.C. Discussion of "Soil Moisture Measurements: Comparison of Instrumentation Performances" by Ventura Francesca, Facini Osvaldo, Piana Stefano, and Rossi Pisa Paola. *J. Irrig. Drain. Res.* **2011**, *137*, 466–468. [CrossRef]
84. Sakaki, T.; Limsuwat, A.; Illangasekare, T.H. A simple method for calibrating dielectric soil moisture sensors: Laboratory validation in sands. *Vadose Zone J.* **2011**, *10*, 526–531. [CrossRef]
85. Friedman, S.P. Soil properties influencing apparent electrical conductivity: A review. *Comput. Electron. Agric.* **2005**, *46*, 45–70. [CrossRef]
86. Archie, G.E. The electrical resistivity log as an aid in determining some reservoir characteristics. *Trans. AIME* **1942**, *146*, 54–62. [CrossRef]
87. Cassiani, G.; Boaga, J.; Rossi, M.; Fadda, G.; Putti, M.; Majone, B.; Bellin, A. Soil-plant interaction monitoring: Small scale example of an apple orchard in Trentino, North-Eastern Italy. *Sci. Total Environ.* **2016**, *543*, 851–861. [CrossRef] [PubMed]
88. Ortuani, B.; Chiaradia, E.A.; Priori, S.; L'Abate, G.; Canone, D.; Comunian, A.; Giudici, M.; Mele, M.; Facchi, A. Mapping soil water capacity through EMI survey to delineate site specific management units within an irrigated field. *Soil Sci.* **2016**, *181*, 252–263. [CrossRef]
89. Deidda, G.P.; Fenu, C.; Rodriguez, G. Regularized solution of a nonlinear problem in electromagnetic sounding. *Inverse Probl.* **2014**, *30*, 125014. [CrossRef]
90. Díaz De Alba, P.; Rodriguez, G. Regularized inversion of multi-frequency EM data in geophysical applications. In *Trends in Differential Equations and Applications*; Ortegón, F., Gallego, M.V., Redondo, N., Rodríguez Galván, J.R., Eds.; SEMA SIMAI Springer Series; Springer: Cham, Switzerland, 2016; Volume 8, pp. 357–369.
91. Shanahan, P.W.; Binley, A.; Whalley, W.R.; Watts, C.W. The Use of Electromagnetic Induction to Monitor Changes in Soil Moisture Profiles beneath Different Wheat Genotypes. *Soil Sci. Soc. Am. J.* **2015**, *79*, 459–466. [CrossRef]
92. Boaga, J. The use of FDEM in hydrogeophysics: A review. *J. Appl. Geophys.* **2017**, *139*, 36–46. [CrossRef]

93. Everett, M.E.; Meju, M.A. Near-surface controlled-source electromagnetic induction: Background and recent advances. In *Hydrogeophysics*; Rubin, Y., Hubbard, S.S., Eds.; Springer: New York, NY, USA, 2005; pp. 157–183.
94. Binley, A.; Kemna, A. DC resistivity and induced polarization methods. In *Hydrogeophysics*; Rubin, Y., Hubbard, S.S., Eds.; Springer: New York, NY, USA, 2005; pp. 129–156.
95. Binley, A.M.; Cassiani, G.; Deiana, R. Hydrogeophysics—Opportunities and Challenges. *Boll. Geofis. Teor. Appl.* **2010**, *51*, 267–284.
96. Cassiani, G.; Bruno, V.; Villa, A.; Fusi, N.; Binley, A.M. A saline trace test monitored via time-lapse surface electrical resistivity tomography. *J. Appl. Geophys.* **2006**, *59*, 244–259. [CrossRef]
97. Constable, S.C.; Parker, R.L.; Constable, C.G. Occam's Inversion: A practical algorithm for generating smooth models from EM sounding data. *Geophysics* **1987**, *52*, 289–300. [CrossRef]
98. La Brecque, D.J.; Heath, G.; Sharpe, R.; Versteeg, R. Autonomous monitoring of fluid movement using 3-D electrical resistivity tomography. *J. Environ. Eng. Geophys.* **2004**, *9*, 167–176. [CrossRef]
99. Cassiani, G.; Godio, A.; Stocco, S.; Villa, A.; Deiana, R.; Frattini, P.; Rossi, M. Monitoring the hydrologic behaviour of a mountain slope via time-lapse electrical resistivity tomography. *Near Sur. Geophys.* **2009**, *7*, 475–486. [CrossRef]
100. Hinnell, A.C.; Ferré, T.P.A.; Vrugt, J.A.; Huisman, J.A.; Moysey, S.; Rings, J.; Kowalsky, M.B. Improved extraction of hydrologic information from geophysical data through coupled hydrogeophysical inversion. *Water Resour. Res.* **2010**, *46*. [CrossRef]
101. Beff, L.; Günther, T.; Vandoorne, B.; Couvreur, V.; Javaux, M. Three-dimensional monitoring of soil water content in a maize field using Electrical Resistivity Tomography. *Hydrol. Earth Syst. Sci.* **2013**, *17*, 595–609. [CrossRef]
102. Garré, S.; Coteur, I.; Wongleecharoen, C.; Kongkaew, T.; Diels, J.; Vanderborght, J. Non-invasive monitoring of soil water dynamics in mixed cropping systems: A case study in Ratchaburi Province, Thailand. *Vadose Zone J.* **2013**, *12*. [CrossRef]
103. Slater, L.; Binley, A.M.; Daily, W.; Johnson, R. Cross-hole electrical imaging of a controlled saline tracer injection. *J. Appl. Geophys.* **2000**, *44*, 85–102. [CrossRef]
104. Cassiani, G.; Binley, A. Modeling unsaturated flow in a layered formation under quasi-steady state conditions using geophysical data constraints. *Adv. Water Resour.* **2005**, *28*, 467–477. [CrossRef]
105. Linde, N.; Binley, A.; Tryggvason, A.; Pedersen, L.B.; Revil, A. Improved hydrogeophysical characterization using joint inversion of cross-hole electrical resistance and ground-penetrating radar traveltime data. *Water Resour. Res.* **2006**, *42*. [CrossRef]
106. Binley, A.; Cassiani, G.; Middleton, R.; Winship, P. Vadose zone flow model parameterisation using cross-borehole radar and resistivity imaging. *J. Hydrol.* **2002**, *267*, 147–159. [CrossRef]
107. Zuecco, G.; Borga, M.; Penna, D.; Canone, D.; Previati, M.; Ferraris, S. Towards improved understanding of land use effect on soil moisture variability: Analysis and modeling at the plot scale. *Procedia Environ. Sci.* **2013**, *19*, 456–464. [CrossRef]
108. Baudena, M.; Bevilacqua, I.; Canone, D.; Ferraris, S.; Previati, M.; Provenzale, A. Soil water dynamics at a midlatitude test site: Field measurements and box modeling approaches. *J. Hydrol.* **2012**, *414*, 329–340. [CrossRef]
109. Jones, S.B.; Wraith, J.M.; Or, D. Time domain reflectometry measurement principles and applications. *Hydrol. Processes* **2002**, *16*, 141–153. [CrossRef]
110. Doolittle, J.A.; Minzenmayer, F.E.; Waltman, S.W.; Benham, E.C.; Tuttle, J.W.; Peaslee, S.D. Ground-penetrating radar soil suitability map of the conterminous United States. *Geoderma* **2007**, *141*, 416–421. [CrossRef]
111. Paniconi, C.; Ferraris, S.; Putti, M.; Pini, G.; Gambolati, G. Three-dimensional numerical codes for simulating groundwater contamination: FLOW3D, flow in saturated and unsaturated porous media. In *Pollution Modeling*; CMP: Boston, MA, USA, 1994; Volume 1, pp. 149–156.
112. Or, D.; Jones, S.B.; VanSchaar, J.R.; Humphries, S.D.; Koberstein, R.L. WinTDR v.6.1: A Windows-based Time Domain Reflectometry Program for Measurement of Soil Water Content and Electrical Conductivity—User Manual. Utah State Univ. Soil Physics Group, Logan. 2004. Available online: https://psc.usu.edu/ou-files/wintdr/Introduction.pdf (accessed on 15 September 2017).
113. Ursino, N.; Cassiani, G.; Deiana, R.; Vignoli, G.; Boaga, J. Measuring and Modelling water related soil—Vegetation feedbacks in a fallow plot. *Hydrol. Earth Syst. Sci.* **2014**, *18*, 1105–1118. [CrossRef]

114. Binley, A. Resistivity Inversion Software. 2013. Available online: http://www.es.lancs.ac.uk/people/amb/Freeware/freeware.htm (accessed on 12 September 2017).
115. Biddoccu, M.; Ferraris, S.; Opsi, F.; Cavallo, E. Long-term monitoring of soil management effects on runoff and soil erosion in sloping vineyards in Alto Monferrato (North-West Italy). *Soil Tillage Res.* **2016**, *155*, 176–189. [CrossRef]
116. Biddoccu, M.; Ferraris, S.; Pitacco, A.; Cavallo, E. Temporal variability of soil management effects on soil hydrological properties, runoff and erosion at the field scale in a hillslope vineyard, North-West Italy. *Soil Tillage Res.* **2017**, *165*, 46–58. [CrossRef]
117. Starr, J.L.; Paltineanu, I.C. Methods for Measurement of Soil Water Content: Capacitance Devices. In *Methods of Soil Analysis: Part 4 Physical Methods*; Dane, J.H., Topp, G.C., Eds.; Soil Science Society of America, Inc.: Madison, WI, USA, 2002; pp. 463–474.
118. Bittelli, M.; Flury, M.; Roth, K. Use of dielectric spectroscopy to estimate ice content in frozen porous media. *Water Resour. Res.* **2004**, *40*, W04212. [CrossRef]
119. He, H.; Dyck, M. Application of multiphase dielectric mixing models for understanding the effective dielectric permittivity of frozen soils. *Vadose Zone J.* **2013**, *12*, 12. [CrossRef]
120. Binley, A.; Ramirez, A.; Daily, W. Regularised image reconstruction of noisy electrical resistance tomography data. In Proceedings of the 4th Workshop of the European Concerted Action on Process Tomography, Bergen, Norway, 6–8 April 1995; pp. 401–410.
121. Monego, M.; Cassiani, G.; Deiana, R.; Putti, M.; Passadore, G.; Altissimo, L. Tracer test in a shallow heterogeneous aquifer monitored via time-lapse surface ERT. *Geophysics* **2010**, *75*, WA61–WA73. [CrossRef]
122. Daily, W.; Ramirez, A.; LaBrecque, D.; Nitao, J. Electrical resistivity tomography of vadose water movement. *Water Resour. Res.* **1992**, *28*, 1429–1442. [CrossRef]
123. Leonard, J.; Andrieux, P. Infiltration characteristics of soils in Mediterranean vineyards in Southern France. *Catena* **1998**, *32*, 209–223. [CrossRef]
124. Ferrero, A.; Usowicz, B.; Lipiec, J. Effects of tractor traffic on spatial variability of soil strength and water content in grass covered and cultivated sloping vineyard. *Soil Till. Res.* **2005**, *84*, 127–138. [CrossRef]
125. Robinson, D.A.; Binley, A.; Crook, N.; Day-Lewis, F.D.; Ferré, T.P.A.; Grauch, V.J.S.; Knight, R.; Knoll, M.; Lakshmi, V.; Miller, R.; et al. Advancing process-based watershed hydrological research using near-surface geophysics: A vision for, and review of, electrical and magnetic geophysical methods. *Hydrol. Process.* **2008**, *22*, 3604–3635. [CrossRef]

© 2017 by the authors. Licensee MDPI, Basel, Switzerland. This article is an open access article distributed under the terms and conditions of the Creative Commons Attribution (CC BY) license (http://creativecommons.org/licenses/by/4.0/).